JGR Atmospheres

Key Points:
- The long-term variabilities in arctic mesosphere and lower thermosphere winds in response to potential climate forcings have been investigated for 1999–2022 over Esrange
- The variability in U and V significantly correlated with O_3 in winter and early spring, and with CO_2 in summer based on altitude
- The interannual variability in U and V is found to vary with altitude and month or season

Correspondence to:

K. Ramesh,
karanamram@gmail.com;
ramara@bas.ac.uk

Long-Term Variability and Tendencies in Mesosphere and Lower Thermosphere Winds From Meteor Radar Observations Over Esrange (67.9°N, 21.1°E)

K. Ramesh[1] , **Nicholas J. Mitchell[1,2]**, **Neil P. Hindley[3]**, and **Tracy Moffat-Griffin[1]**

[1]British Antarctic Survey (BAS), Cambridge, UK, [2]Centre for Atmospheric and Environment Research, University of Bath, Bath, UK, [3]Centre for Climate, Adaptation and Environment Research, University of Bath, Bath, UK

Abstract Long-term variabilities of monthly zonal (U) and meridional winds (V) in northern polar mesosphere and lower thermosphere (MLT, ∼80–100 km) are investigated using meteor radar observations during 1999–2022 over Esrange (67.9°N, 21.1°E). The summer (June-August) mean zonal winds are characterized by westward flow up to ∼88–90 km and eastward flow above this height. The summer mean meridional winds are equatorward with strong jet at ∼85–90 km and it weakens above this height. The U and V exhibit strong interannual variability that varies with altitude and month or season. The responses of U and V anomalies (from 1999 to 2003) to solar cycle (SC), Quasi Biennial Oscillation at 10 and 30 hPa, El Niño-Southern Oscillation, North Atlantic Oscillation, ozone (O_3) and carbon dioxide (CO_2) are analyzed using multiple linear regression. From analysis, significant regions of correlations between MLT winds and above potential drivers vary with altitude and month. The positive responses of U and V to SC (up to 15 m/s/100 sfu) indicates the strengthening of eastward winds in mid-late winter, and poleward winds in late autumn and early winter. The O_3 likely intensifies the eastward and poleward winds (∼100 m/s/ppmv) in winter and early spring. The CO_2 significantly influence the eastward flow in late winter and summer (above ∼90–95 km) and strengthen the meridional circulation. The significant positive trend in U peaks in summer, late autumn and early winter (∼0.6 m/s/year), the negative trend in V is more prominent in summer above ∼90–95 km.

Plain Language Summary The transition region between middle atmosphere and thermosphere is known as the mesosphere and lower thermosphere (MLT). The dynamics and circulation in this region are significant for global transport of important trace chemical species. Further the MLT winds play crucial role for the dynamical coupling of the middle and upper atmosphere. In the present study, the long-term variability and tendencies in monthly mean zonal and meridional winds are investigated in the Arctic MLT between ∼80 and ∼100 km from meteor radar observations during 1999–2022 over Esrange (67.9°N, 21.1°E) in Sweden. The ability of radar provided the unique, consistent, and long-term data set of polar MLT winds for duration of about two solar cycles. The MLT winds show important characteristic features and significant interannual variability that vary with altitude and month or season. In addition, the possible influence of climate forcings viz., solar activity, Quasi Biennial Oscillation (at 10 and 30 hPa), El Niño-Southern Oscillation, North Atlantic Oscillation, ozone, and carbon dioxide on the variabilities of polar MLT winds has been analyzed using multiple linear regression. The significant interannual variabilities and tendencies in northern polar MLT zonal and meridional winds can be attributed to the above potential drivers.

1. Introduction

The mesosphere and lower thermosphere (MLT) is a complex transitional region of the terrestrial middle and upper atmospheres with the interactive dynamical processes dominated by gravity waves (GWs), planetary waves (PWs) and tides. The MLT winds are significantly driven by these waves as they break, and deposit energy and momentum carried from the lower atmosphere. The mean meridional circulation driven by GW drag has great impact on temperature and altitude of the mesopause, particularly over polar latitudes establishing colder, lower in summer, and warmer, higher in winter (e.g., Andrews et al., 1987; Fritts & Alexander, 2003; Garcia & Solomon, 1985; Haurwitz, 1961; Holton, 1982, 1983; Lindzen, 1981; Lübken & von Zahn, 1991; Smith, 2012; von Zahn et al., 1996; Xu et al., 2007). The MLT winds/circulation play vital role in the global distribution of important chemical species like NO, CO, and CO_2 (e.g., Marsh & Roble, 2002; Smith et al., 2011). The MLT comprises coupling of atmospheric layers with various physical properties. The energy balance between forcings

from below and above vary according to the magnitudes of the perturbations (Smith et al., 2017). The neutral winds of this region can have primary impact on the space-weather effects in the ionosphere (e.g., Jackson et al., 2019; Sassi et al., 2019).

The 11-year solar cycle (SC) signatures can be seen in the MLT region (e.g., Ramesh et al., 2015). Apart from the temperature, the horizontal winds in the MLT/mesopause region depends on the solar activity (Bremer et al., 1997; Greisiger et al., 1987). The zonal and meridional winds can be positively correlated (based on season) with the SC in response to changes in thermal and dynamical structures of the stratosphere that impact the upward propagating GWs and thereby the MLT winds (e.g., Cai et al., 2021). Cullens et al. (2016) simulated the responses of GWs, and wave-driven circulations to the SC. They showed that the significant changes in GW drag and associated residual circulation/MLT winds could be due to 11-year SC variability over the southern polar latitudes. Wilhelm et al. (2019) used meteor radar observations to characterize the MLT winds over Andenes (69.3°N, 16°E). They found that the mean winds exhibit a characteristic season dependent 11-year SC effect in the Arctic MLT. The observations of the MLT wind variability at SC periods are still tentative due to limited data sets, and difficulty to identify small changes. The modeling studies like Qian et al. (2019) emphasizes the significant impact of the solar activity on the MLT winds, variable in spatial and temporal domains.

Any peculiar changes in the troposphere and stratosphere can largely affect the thermal and dynamical structures of the MLT. The major disturbances include wintertime sudden stratospheric warmings (SSW) to temporarily disrupt the MLT circulation and temperatures (Sathishkumar et al., 2009; Vincent, 2015). The large variability associated with the dynamical properties of the SSW events is evidenced in the MLT region from various experimental observations and model simulations. The weakening/reversal of westward winds accompanied by cooling at high latitude MLT are mainly associated with the PW and GW forcings (e.g., Chau et al., 2012; Hoffmann et al., 2007; Yamazaki et al., 2020). The Quasi-Biennial Oscillation (QBO) is a predominant dynamical variability in the equatorial stratospheric ($\sim$16–50 km) zonal winds, characterized by downward propagating eastward and westward wind regimes with a variable period averaging $\sim$27–28 months (e.g., Baldwin et al., 2001; Reed et al., 1961). The effect of the QBO can be observed globally through dynamical coupling (by interaction of QBO with GWs and PWs) between the tropical lower stratosphere and the global middle atmosphere (e.g., Baldwin & Dunkerton, 1998; Dunkerton & Baldwin, 1991) including the MLT (e.g., Ford et al., 2009; Jacobi et al., 1996; Hibbins et al., 2007). The dependence of SSW occurrence on QBO phase can be found in Salminen et al. (2020). They confirmed that the SSWs occur more often in easterly QBO phase than in westerly phase.

The El Niño-Southern Oscillation (ENSO) is one of the key variabilities to influence the MLT winds, temperature and tidal structure (e.g., Gurubaran et al., 2005; Lieberman et al., 2007; H. Liu et al., 2017; Warner & Oberheide, 2014). It is a coupled atmosphere and ocean phenomenon with irregular periodic (2–7 years) warming in sea surface temperatures over the equatorial eastern and central eastern Pacific Ocean. More details on ENSO can be found in Scaife et al. (2019). The response due to ENSO includes perturbations in the tropospheric convection that influences the tidal forcing and yield variability in tidal amplitudes and subsequently the winds and temperature in the MLT region (e.g., Ramesh et al., 2020a, 2020b). The North Atlantic oscillation (NAO) which is closely related Northern Annular Mode, is another dominant driver of the atmospheric variability (e.g., Kolstad et al., 2020) that connects the polar stratosphere and mesosphere via dynamical coupling (e.g., Jacobi & Beckmann, 1999). Although it is the regional scale tropospheric circulation over Atlantic and Europe, the connection between NAO and stratospheric polar vortex could be useful for the detection of long-term variability in the MLT winds over this region.

The anthropogenic increase in greenhouse gases, particularly CO_2 not only influencing the lower atmospheric climate but also the middle and upper atmospheric processes. The rising levels of CO_2 propagate upward due to advective transport and eddy vertical mixing by GWs (e.g., Emmert et al., 2012; Garcia & Solomon, 1985; Garcia et al., 2014; Qian et al., 2017; Rezac et al., 2015; Shia et al., 2006; Yue et al., 2015) and significantly influence the thermal structure through radiative cooling and thereby the dynamical processes, composition and chemical reactions in the MLT. The zonal winds are linked to the temperature gradients in near agreement with the thermal wind balance (Andrews et al., 1987), the exact balance can differ as it is also significantly influenced by the strong dynamical forcings in the MLT. Thus, the changes in temperature and minor species accompanied by increasing CO_2 have direct impact on variabilities in the MLT winds (e.g., Laštovička et al., 2008), however the knowledge of its long-term effects is inadequate. Ozone also plays a significant role for the changes in the MLT temperature and winds. It strongly affects the stratospheric temperature and in turn the winds that alter the spectrum of GWs

reaching the MLT (e.g., Venkateswara Rao et al., 2015) and hence the winds there. Furthermore, as it is crucial for generating atmospheric tides through solar heating, any changes in stratospheric ozone greatly impact the propagation characteristics of the tides that effectively modulate the winds in the MLT region. The trends and changes in mesosphere/mesopause ozone and their consequences are least explored (Laštoviĉka et al., 2008).

From the above studies, it is evidenced that the MLT winds are significantly modulated by the solar forcing and lower atmospheric perturbations. Most of the studies on long-term tendencies in the MLT winds are from equatorial/low-latitudes (Burrage et al., 1996; Gurubaran & Rajaram, 1999; Kishore Kumar et al., 2014; Rajaram & Gurubaran, 1998; Sridharan et al., 2007, 2010; Venkateswara Rao et al., 2012) along with short-term variabilities (K. K. Kumar et al., 2007, 2008; Rao et al., 2014), and mid-latitudes (Jacobi, 2012; Jacobi et al., 2005, 2012, 2015; Namboothiri et al., 1993, 1994; Portnyagin et al., 2006); however the trends and variabilities in the high-latitude (including Arctic and Antarctic) MLT winds are very limited (Baumgaertner et al., 2005; Dempsey et al., 2021; Dutta & Sridharan, 2023; Hindley et al., 2022; Jaen et al., 2023; Lukianova et al., 2015, 2018; Mitchell et al., 2002; Venkateswara Rao et al., 2015) from various observations and model simulations. Global variabilities in the MLT winds can be found at Ramesh et al. (2020a), X. Liu et al. (2023) and references therein.

The MLT winds can be investigated mostly based on remote sensing techniques. Although space-borne observations provide near global picture, radars are efficient ground-based tools for measuring the MLT winds with good height and time resolutions. The meteor radars, that use the reflection of radio waves by meteor trails (e.g., Mitchell et al., 2002), are widely used for continuous measurements of the MLT winds (e.g., K. K. Kumar et al., 2007; Rao et al., 2014; Lukianova et al., 2018 to state a few). The medium frequency (MF) radars also measure the MLT winds but based on the reflections by changes in the refractive index (e.g., Gurubaran et al., 2007; Vincent et al., 1998). Both meteor and MF radars provide continuous horizontal wind measurements in the height region of ∼70–100 km, however the MF radars are believed to underestimate the winds above ∼90 km in the MLT region (Hall et al., 2005; Manson et al., 2004; Wilhelm et al., 2017).

The polar MLT is very complex because of the distinctive features like auroral and geomagnetic activities, energetic particle precipitation, coldest part of the terrestrial atmosphere (summer mesopause), pole-to-pole mean residual circulation, noctilucent clouds (NLCs) and associated summer/winter echoes, effects of polar vortex and SSWs, stratospheric ozone hole etc. Hence understanding the dynamics of the MLT, its long-term variability and response to external perturbations is critical to explore the coupling of the middle and upper boundary of the terrestrial atmosphere. The main purpose of this study is to investigate, for the first time, the long-term tendencies and interannual variabilities in Arctic MLT zonal and meridional winds over Esrange (67.9°N, 21.1°E) under the influence of the most significant drivers viz., solar activity, QBO (at 10 and 30 hPa), ENSO, NAO, O_3, and CO_2. A multiple linear regression (MLR) model is used with the above forcings to investigate the potential drivers of the variability and tendencies in the MLT winds using the meteor radar observations for 1999–2022 (two SCs) over Esrange. Section 2 provides the details of data and analysis method, Section 3 presents the results, summary and discussion are elaborated in Section 4 and finally the important conclusions of the study are listed in Section 5.

2. Data and Analysis Method

2.1. Meteor Radar Observations Over Esrange

The meteor radar used in this study is an all-sky Interferometric SKiYMET VHF system that was installed in August 1999 at Esrange (67.9°N, 21.1°E), nearly 30 km east of Kiruna in Sweden. This is believed to have been the first meteor radar equipped with height-finding ability to be permanently deployed in the Arctic. The radar is a pulsed system that uses a transmitter with a peak power of 6 kW. It operates at a radio frequency of 32.5 MHz, a pulse repetition frequency of 2,144 Hz, and a duty cycle of 15%. The system uses crossed-element Yagi antennas for both transmit and receive to allow a detection of meteor echoes at all azimuths. There is a single transmitter antenna and an array of five receiver antennas which form an interferometer to enable determination of meteor-echo zenith and azimuth angles. The height and time resolutions for routine wind measurements are ∼2 km and 1 hr, respectively. This radar configuration has remained essentially unchanged since the system was installed—which makes it well suited to long-term studies because it greatly reduces the possibility of measurement biases that might otherwise arise from any major changes in the system hardware.

The performance of Esrange meteor radar has been carefully investigated to determine if there is any significant change over the duration of the data set, as it is an essential step in the studies of long-term variability. A particular interest was to see if there was any evidence of damage to the interferometer that might result in greater errors or biases in meteor height estimations and thus in the derived winds. The average altitude of the meteor echoes in each month (Figure S1 in Supporting Information S1) is consistent between ∼88 and ∼91 km throughout the observational period. Further it is in phase with the 11-year SC as revealed in a recent study of the long-term variability in the heights of meteor echoes (Dawkins et al., 2023), that investigated data from 12 meteor radars (including the Esrange radar used in this study) and showed both linear and 11-year variations in peak meteor height. The peak heights decreased at all sites and a positive correlation with solar activity was observed at most sites; however, at high latitudes an anticorrelation was observed. Note that the magnitude of these variations is relatively small compared to the ∼20 km depth of the meteor region and so will have little impact on the ability of the radar measurements to determine the MLT winds at ∼80–100 km. In any study of the inter-annual variability of the MLT winds, it is essential to know that any apparent variability detected is a property of the atmosphere and not an artifact caused by possible changes or drift in the performance/biases of the radar. In the case of the Esrange meteor radar, as noted above, there have been no significant changes to the hardware of the system. Therefore, valid comparisons can be made between the winds deduced from meteor radar observations over the duration of the data set. A complete description of the design of this type of radar and the meteor detection algorithm can be found in Hocking et al. (2001). The data collection over Esrange commenced on 5 August 1999 and since then the radar has been in operational mode till date (in 2023), with several data gaps arising due to technical issues and when the radar was inoperable. The data availability and gaps can be found in Figure S2 in Supporting Information S1. However, the present study uses the data recorded up to the end of year 2022. Note that here the radar refers to "Esrange meteor radar," but it has been sometimes referred to as the "Kiruna meteor radar" in existing literature.

2.2. Methodology

2.2.1. Gaussian-Weighted Method for Meteor Radar Winds

The present study adopts the improved time-height localization of meteor radar winds using a Gaussian-weighting method developed by Hindley et al. (2022). This method significantly improves the accuracy in deriving the horizontal winds for irregular meteor distributions in time and height, when compared to a conventional height gates approach (e.g., Mitchell et al., 2002). For a particular time-height location, instead of binning meteor echoes into time-height bins, the method uses a Gaussian-weighted least squares fit (see Hindley et al., 2022, Equations 1–3) based on all meteors within two standard deviations to estimate the zonal (U) and meridional (V) wind components at the weighted time-height location of the meteor echoes considered.

The advantages of Gaussian weighting approach over a fixed height gates method are (a) full altitude coverage of reliable winds can be achieved during higher meteor counts for some cases like local mornings, (b) the derived winds are correctly attributed to the weighted average time-height location of the available meteors, and (c) derived winds are highly resistant to anomalous values when meteor counts are low because they are constrained with meteors from adjacent heights and times, which are not used in a fixed binning approach. Further details on the Gaussian weighting method for deriving the meteor radar winds used in this study can be obtained from Hindley et al. (2022).

2.2.2. Multiple Linear Regression

The long-term variability and tendencies in Arctic monthly MLT winds in response to the potential climate forcings are determined through MLR analysis for 1999–2022. The mean changes in monthly winds and predictors are calculated with respect to the first 5 years of observations as the difference of the value for each month from the average over the period 1999–2003. The MLR analysis on the changes in zonal (ΔU) and meridional wind (ΔV) determines the response associated with the SC, QBO, ENSO, NAO, O_3, and CO_2. The typical expression for regression model can be given as follows.

$$\alpha(t) = \emptyset + \sum_{k=1}^{n} \beta_k M_k(t) + \varepsilon(t) \tag{1}$$

where α is the predictand, that is, dependent variable, ΔU or ΔV, t is the time in months/years, $\varnothing$ is a constant, β_k are regression coefficients corresponding to n predictors (here $n = 7$), M is a matrix containing n predictors, and ε is the residual. The regression analysis uses seven predictors that have potential impact on variabilities in Arctic MLT winds. Here the matrix M consists of the following seven predictors:

$$M = \begin{pmatrix} F_{10.7} \\ QBO10 \\ QBO30 \\ NINO\ 3.4 \\ NAO \\ O_3 \\ CO_2 \end{pmatrix} \quad (2)$$

where.

(i) $F_{10.7}$ is the 10.7 cm solar radio flux. It is a proxy for solar activity in solar flux units (sfu) with 1 sfu $= 10^{-22}$ Wm^{-2} Hz^{-1}. The monthly $F_{10.7}$ values are obtained from https://lasp.colorado.edu/lisird/data/cls_radio_flux_f107/.

(ii) QBO10 and QBO30 are the zonal mean zonal winds (m/s) averaged over 5°N–5°S at 10 and 30 hPa respectively for QBO. The European Center for Medium-range Weather Forecast Reanalysis version 5 (ERA5) data of zonal winds are used for the QBO. The ERA5 reanalysis zonal winds on 10 and 30 hPa pressure levels are downloaded from the ECMWF archive: https://cds.climate.copernicus.eu/cdsapp#!/dataset/10.24381/cds.bd0915c6?tab=overview

(iii) NINO 3.4 index, the proxy for ENSO, is equatorial Pacific Sea surface temperature (K) averaged for 5°N–5°S and 170°W–120°W. The monthly NINO 3.4 index data are obtained from https://psl.noaa.gov/gcos_wgsp/Timeseries/Data/nino34.long.data

(iv) NAO, the North Atlantic Oscillation is the key driver of the climate variability in parts of Eurasia, Greenland, North America, and North Africa. The NAO index is the difference in normalized sea level pressures between Ponta Delgadas (Azores) and Akureyri (Iceland). The NAO index data are downloaded from https://www.cpc.ncep.noaa.gov/products/precip/CWlink/pna/norm.nao.monthly.b5001.current.ascii.table

(v) O_3 is the global mean of monthly ozone mass mixing ratio (MMR) at 1 hPa (~48 km). The ERA5 reanalysis O_3 MMR data is downloaded from https://cds.climate.copernicus.eu/cdsapp#!/dataset/reanalysis-era5-pressure-levels?tab=form. The O_3 MMR has been converted into volume mixing ratio (VMR) in ppmv from

$$VMR\ (ppmv) = \left(\frac{\text{mean molecular weight of dry air (28.9644)}}{\text{molecular weight of } O_3 \text{ (47.9982)}} \right) \times 10^6 \times MMR$$

(vi) CO_2 is the global average of monthly surface carbon dioxide VMR (ppmv). The data is obtained from https://gml.noaa.gov/webdata/ccgg/trends/co2/co2_mm_gl.txt

The MLR analysis uses the regressors of monthly mean changes with respect to 1999–2003 to derive the regression coefficients/response of each predictor. It can be noted that the data gaps are incorporated deliberately in the regressors for the months and years corresponding to that in the radar wind observations (as given in Figure 1f) to avoid misinterpretations of the results obtained from the regression analysis.

3. Results

In this section, the performance evaluation, and data availability of the meteor radar observations for 1999–2022 over Esrange along with the predictors and their responses to ΔU and ΔV are presented.
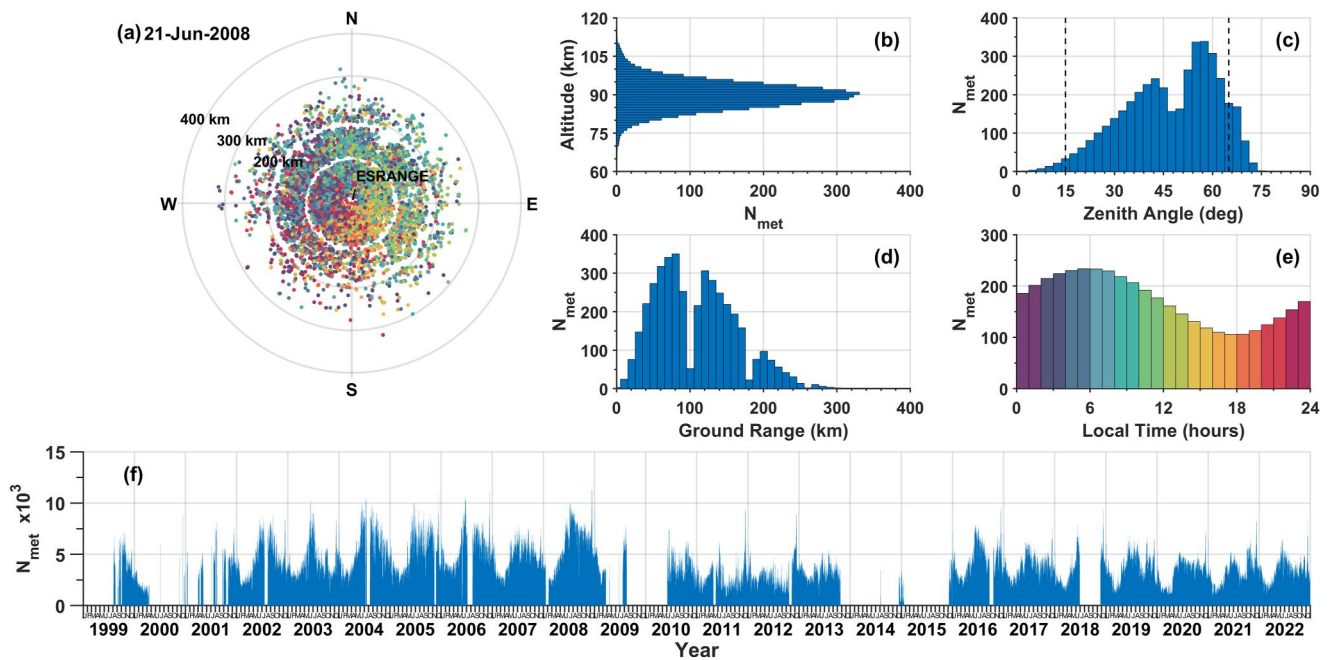
Figure 1. (a) Horizontal distribution of normalized individual meteors recorded around Esrange meteor radar on 21 June 2008. Each meteor echo is denoted by a dot colored according to the time of detection as per the color scale in panel (e); (b) average height distribution of the meteors per day, (c) zenith angle, (d) horizontal (ground) range, (e) local time of all meteor echoes detected per day for all the operational days, (f) daily variation of the number of meteors counts per day during the observational period (1999–2022) over Esrange.

3.1. Meteors Detection and Distribution

Figure 1 shows examples that illustrate various properties of the distribution of meteors recorded by the radar system. Figure 1a presents the location projected onto a horizontal plane of normalized individual meteors recorded around the radar on 21 June 2008. Each meteor is represented by a dot and color-coded to indicate the local time at which it was recorded using the color scale of Figure 1e. As seen, meteors are detected at all azimuths, although there are some biases of azimuths toward certain local times, which is a consequence of the visibility above the horizon of sporadic meteor radiants and the right-angle geometry of line-of-sight and meteor trail required for a meteor to be detected (e.g., J. P. Younger et al., 2009; P. T. Younger et al., 2009). Figure 1b exhibits the average height distribution of the meteors per day (total meteor counts/total number of operational days) for all the operational days during August, 1999–December, 2022. Note the strongly peak distribution with a maximum at ~90 km in association with the neutral density variability that changes by few kilometers based on the season. Very few meteors are detected below 80 km or above 100 km, and so these heights represent a practical limit for routine measurement of winds. Figure 1c shows the measured distribution of zenith angles, which maximizes near ~60°. The meteors in the zenith angles between 15° and 65° (vertical dashed lines in Figure 1c) are used in the present study to avoid errors in the wind measurement near zenith and at large zenith angles.

The distribution of the meteors corresponding to ground range (i.e., projected onto the surface, rather than slant range) has been depicted in Figure 1d. It is apparent that the meteors can be detected up to ~240–300 km with a peak range between 60 and 140 km. Figure 1e illustrates the diurnal variation in hourly meteor counts averaged for the observational period. The observed ratio of maximum to minimum count rates is about 2:1 with a maximum occurring at about 06:00 LT and minimum at about 18:00 LT. This ratio is typical for high latitude sites, and it signifies that there are still enough meteors to estimate the winds even during the low count rate part of the day. The number of meteors counts per day during the observational period are shown in Figure 1f to illustrate the seasonal distribution of meteor detections. Note the data gaps when no meteor radar observations were recorded (as given in Figure S2 in Supporting Information S1). The Figure shows that the daily total meteor counts vary from about 2,500 during winter (December-February) and then start increasing from spring (March-May) to peak at more than 5,000 in summer (June-August), an astronomical variation related to the visibility of
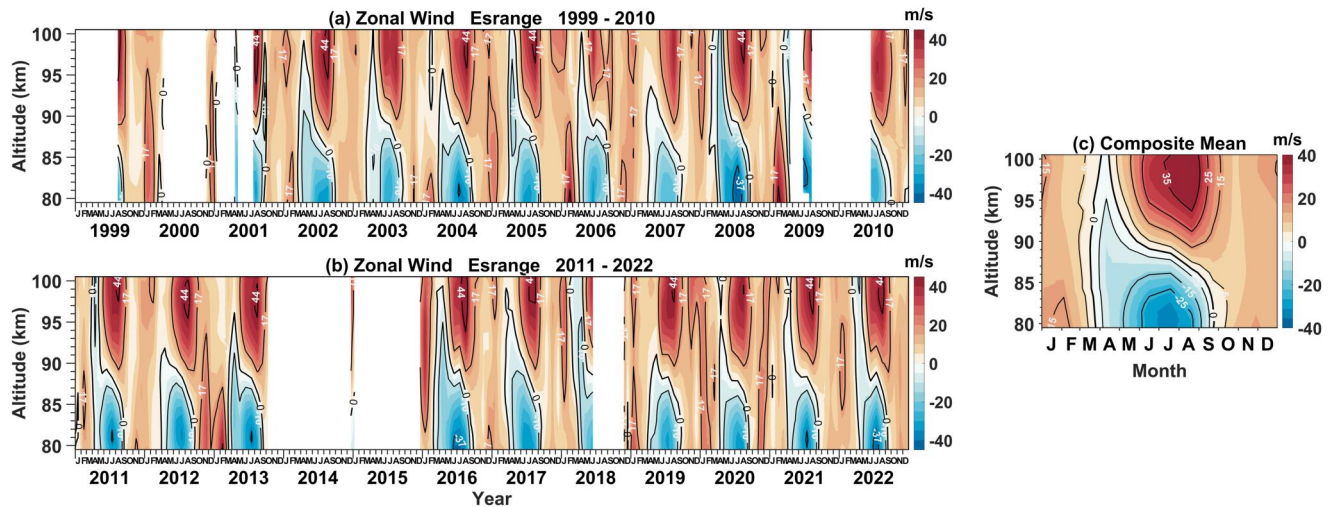
Figure 2. Monthly mean zonal winds for (a) 1999–2010, (b) 2011–2022, and (c) their composite means in the mesosphere and lower thermosphere region (∼80–100 km) from the meteor radar observations over Esrange.

sporadic meteor radiants. Experience (e.g., Hindley et al., 2022; Mitchell et al., 2002) shows that meteor count totals in this range are sufficient to determine zonal and meridional winds with useful height and time resolutions at the heights of ∼80–100 km in the MLT region.

3.2. Climatology of Zonal and Meridional Winds

The variation in monthly mean zonal winds for ∼80–100 km during 1999–2022 over Esrange are presented in Figures 2a and 2b. The vertical white areas represent the data gaps due to non-availability of meteor radar observations. As seen in the figure, there is strong interannual variability in the zonal winds. For example, the summer westward winds range from −25 m/s at ∼80–82 km in 2007 to −40 m/s at the same height in 2008. Similarly, the variation in eastward winds ranges between ∼15 m/s in 2002 and ∼30 m/s in 2012, especially below ∼90 km in autumn and early winter. The zonal winds are mainly characterized by strong westward winds below ∼90 km and reverses to strong eastward above this height in summer (JJA). In addition, the westward winds are also apparent in the spring (MAM) reaching the higher altitudes in some years (e.g., 2003, 2005, 2008, 2011, 2018, 2022). The zonal winds are eastward at all heights in winter (DJF) and during autumn (SON) except in September (above ∼90 km) with relatively stronger winds in winter. Note the stronger winter eastward winds are not consistent across all the years and vary with altitude. The composite mean (average of all years) of monthly zonal winds are shown in Figure 2c for the climatological features of the MLT zonal winds over Esrange. From the figure, it is clear that the summer westward flow is stronger below ∼90 km, a region that represents the top of the westward jet in summer polar mesosphere. Above this height, the summer zonal flow reverses to eastward with maximum speed at around 98 km during July-August. The zonal winds are eastward at all heights in winter with equinoxes being the extended transitions between winter and summer flow through the zero-wind line that descends in summer.

Figures 3a and 3b represent the variabilities in the monthly mean meridional winds between ∼80 and ∼100 km for 1999–2022 over Esrange. The meridional flow is equatorward in summer during all the years with variable speeds at different heights, and strong winds (−15 m/s) mostly at ∼85–90 km. It exhibits significant interannual variability in poleward flow that ranges from ∼5 m/s in 2002 to ∼12 m/s in 2016 below ∼90 km during autumnal equinox and early winter. Further the meridional winds are equatorward in January of certain years, for example, 2006, 2007, 2012; however, they are poleward in some other years like 2008, 2009, 2016, 2022 (at least below ∼90 km). The poleward flow occurs at least for 2 months in autumnal equinox up to ∼90 km, extending to winter in some of the years for example, 2008–2009, 2012–2013, 2020–2021, and 2021–2022. In general, the winter flow is equatorward between poleward wind patterns of the autumnal and spring equinoxes, however this is not consistent for all the years. The composite (mean of all the years) structure of the monthly mean meridional winds is shown in Figure 3c. The meridional flow is characterized by strong equatorward jet centred at ∼85–90 km
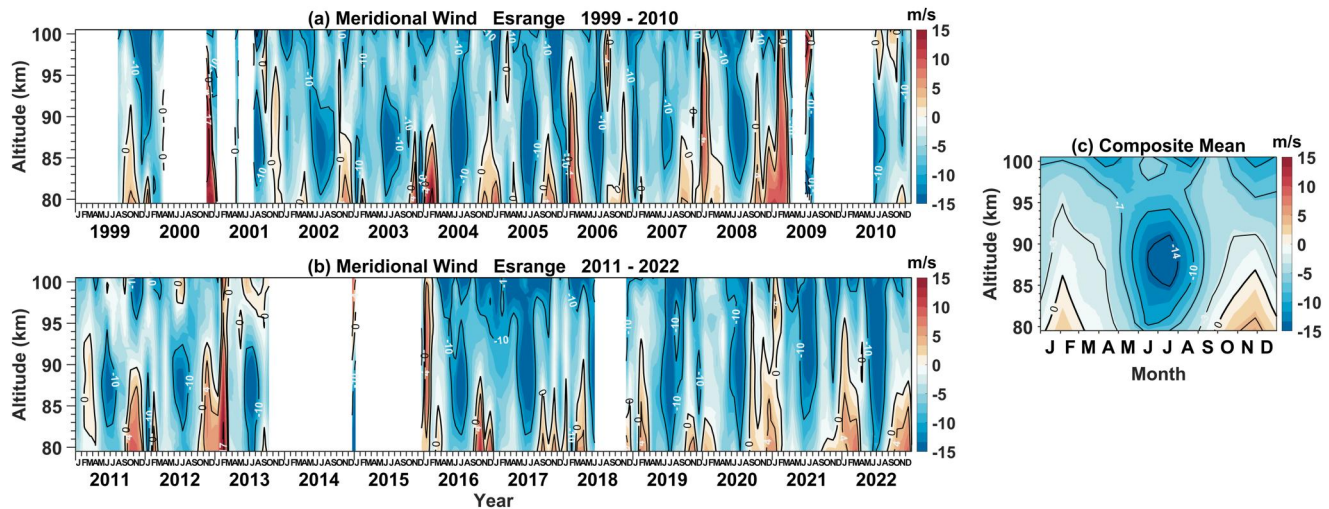
Figure 3. Same as Figure 2 but for meridional winds.

summer, however it weakens above this height. The equinoctial poleward winds are merged into part of the winter months, and they extend with height up to ∼86 km.

3.3. Interannual Variabilities of Zonal and Meridional Winds

The interannual variabilities of the zonal (U) and meridional winds (V) for each month at two different (lower and upper) heights, 82.3, and 98.5 km for 1999–2022 are shown in Figure 4. The white pixel regions in the figure represent the data gaps. There is substantial interannual variability in zonal and meridional winds observed in each month at two height regions. It is obvious in zonal winds during June-August at 82.3 km where the summer westward flow is maximum. In June, the westward wind speed ranges from ∼15 m/s in 2002 to ∼50 m/s in 2009 and consistent at ∼25 m/s for consecutive years during 2004–2006 and 2021–2022. Similarly in the months of July and August, there is a significant year-to-year variability of the westward winds. Besides, the large variability of the eastward winds can be observed in winter months. In January, the eastward wind speed ranges from ∼5 m/s in 2001 to ∼30 m/s in 2000, 2005, 2019 and consistent as ∼10 m/s in 2002–2004, 2006, 2008–2009, and 2018. In February, the eastward wind speeds vary from a maximum of ∼50 m/s in 2006, 2009, and 2013 to the minimum of ∼5 m/s in 2003, 2005, 2007, 2017–2019, and 2021–2022. Likewise, the zonal winds exhibit prominent year-to-year variability during the transition periods of equinoxes. At 98.5 km where the summer eastward flow peaks, the maximum eastward wind speeds above ∼50 m/s can be found in August of 1999, 2001–2002, 2005, 2012, 2016, and 2021–2022, and the minimum of ∼10–20 m/s in 2006 and 2014. However, in recent years, the peak eastward winds attain ∼40 m/s in the month of July. Further, the year-to-year variability is more prominent in winter solstice and equinoxes.

In the case of meridional winds, the summer equatorward flow exhibits prominent year to year variability at 82.3 km. For example, in June-July, the equatorward wind speed varies from maximum of 15 m/s in 2004–2005 to around 10 m/s in 2017 and 2021 and so on. The reversal of equatorward and poleward winds can be noticed in winter and equinoxes respectively in certain years, for example, 2000, 2009, 2016, 2022 in December-January (poleward) and 2003, 2012, 2017 in March and September (equatorward). At 98.5 km, the interannual variability of meridional winds are more pronounced in all the months. The equatorward winds are evidenced in almost all the years except during 2009–2013 in June-July. Besides, the winter equatorward wind reversal to poleward can be observed in December of 2014, and in 2008, 2009, 2013, 2016, 2021 during January-February. During equinoxes, the year-to-year variability is more prominent for the equatorward winds including reversal to poleward in March of 2005, in September of 2001, 2010–2011, 2013, 2020, and during October in 2010.

Figure 5 shows the composite mean of all years for the monthly zonal and meridional winds to characterize the interannual variabilities at two heights of 82.3 and 98.5 km (blue lines). The red vertical bars in each panel represent the corresponding standard deviations for each month to signify the variabilities in winds. At 82.3 km, the interannual variability of the zonal winds is more pronounced in winter eastward winds especially in February
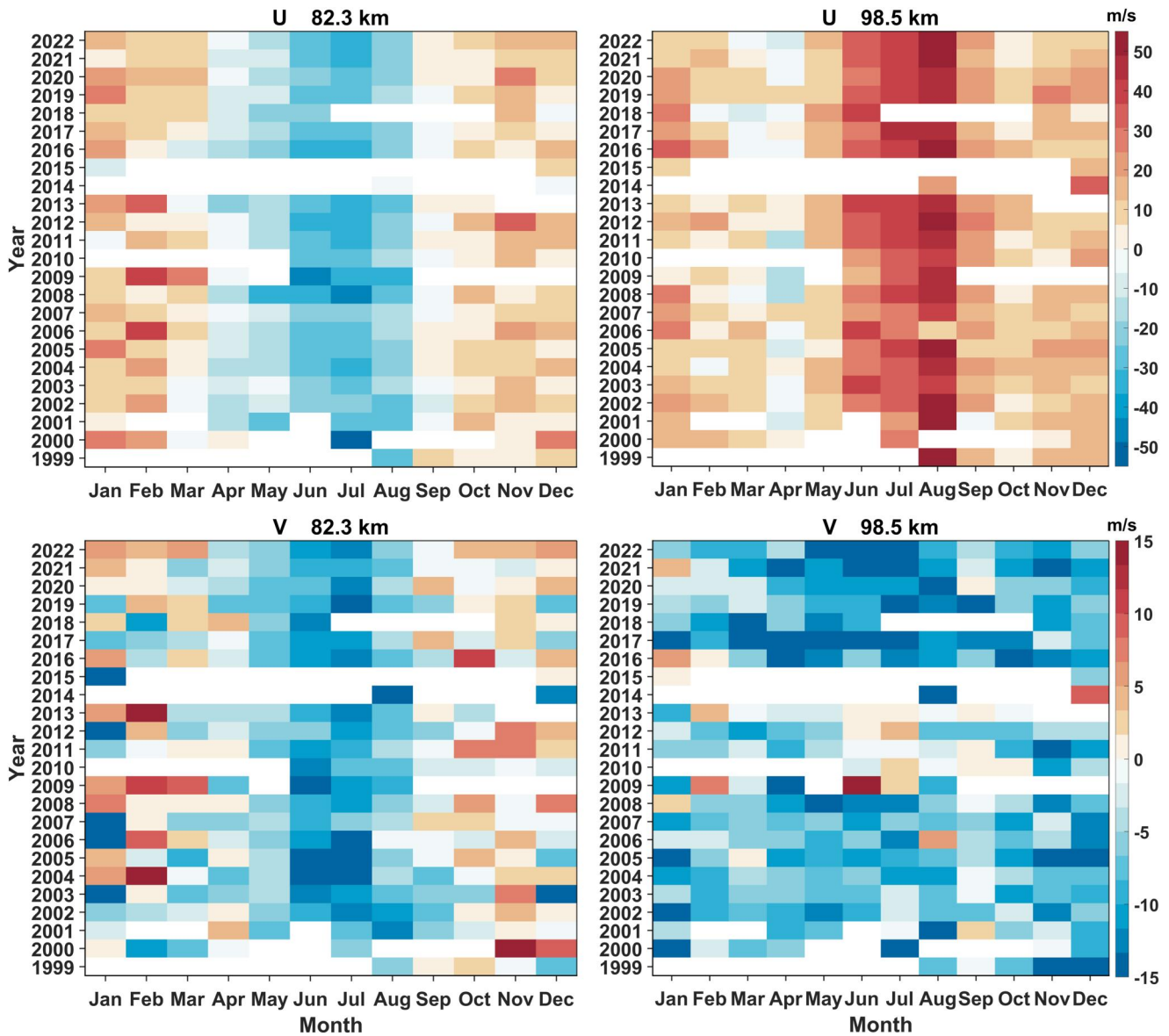
Figure 4. Year-to-year variability of (top) zonal and (bottom) meridional winds for each month at two different heights of (left) 82.3 km and (right) 98.5 km during 1999–2022 over Esrange.

(∼12 m/s) and least in autumnal equinox (∼3.5 m/s). In summer, the maximum deviation in westward winds occurs in July (∼6.8 m/s). At 98.5 km, the variability in eastward winds is maximum in August (∼11 m/s) and minimum in May and October (∼4 m/s). For the meridional winds at 82.3 km, the large variability can be found during winter with maximum for equatorward winds in January (∼8.4 m/s) and poleward winds in February (∼7.6 km), however it is minimum for equatorward winds in May (∼1.3 m/s). At 98.5 km, the interannual variability of the meridional winds is considerably larger in almost all the months, however it is maximum primarily in summer (∼6–9 m/s) and then in winter (∼5–7 m/s).

3.4. Time Series of Predictors

The temporal variations of the climate forcings (predictors) used in the regression analysis (defined in Section 2) are given in Figure 6. The figure includes the monthly mean of the proxies viz., $F_{10.7}$, QBO10, QBO30, NINO 3.4 index, NAO index, O_3 and CO_2 for 1999–2022. The $F_{10.7}$ index includes 23rd, 24th, and part of 25th 11-year SCs with declining solar maxima. The QBO10 and QBO30 zonal winds vary up to 20 m/s in eastward and 40 m/s in
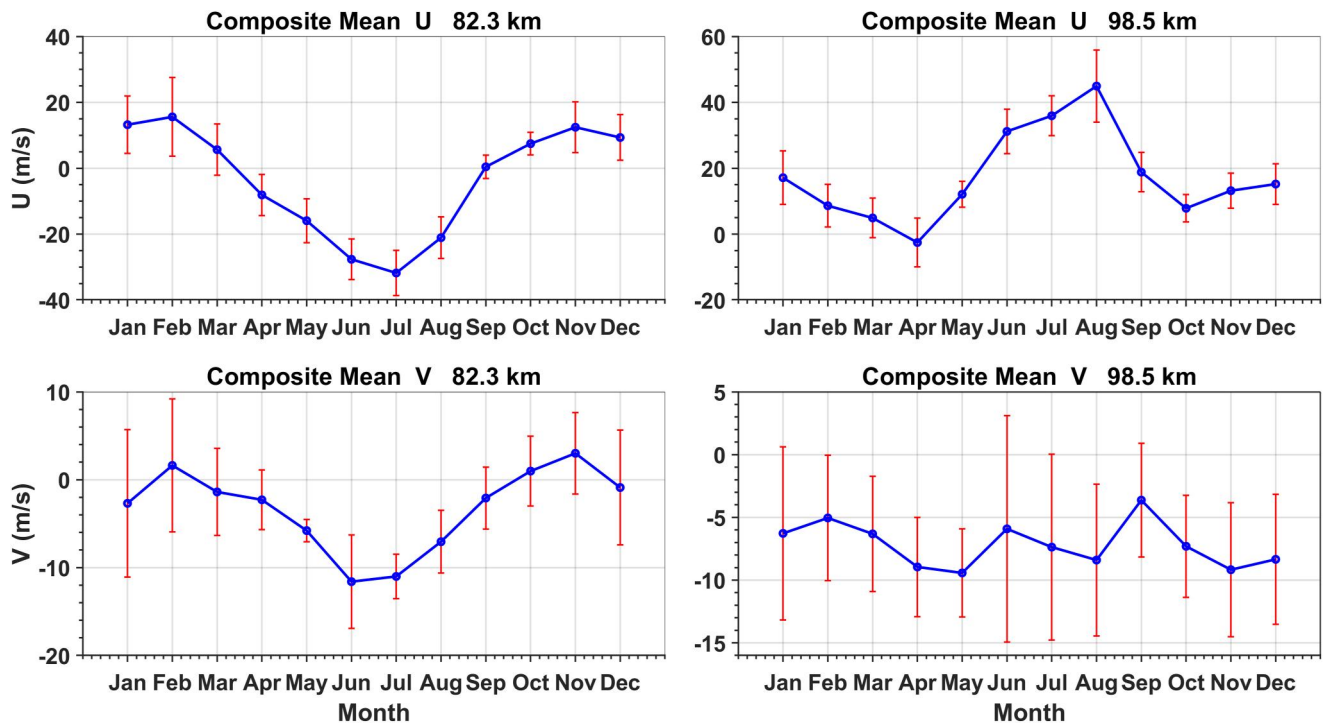
Figure 5. Monthly variation of composite means of (top) zonal, and (bottom) meridional winds (in blue) at two different heights, (left) 82.3 km and (right) 98.5 km. The vertical bars (in red) represent the standard deviations of the winds for each month.

westward. The are no long-term trends evident in both QBO indices. The two indices for QBO (at 10 and 30 hPa) used in the MLR analysis are approximately in quadrature and the selection of these two follows the analysis of Randel and Wu (1996, 2007) to acquire all possible responses of the QBO. The proxy for ENSO, the NINO 3.4 index shows slight increasing trends during 2011–2015 in consistent with warming in the sea surface temperature anomalies. However, in recent years, the small decreasing trend in NINO 3.4 index indicates the reduction in the ENSO variability. The NAO, also influenced by interaction with ENSO in winter, doesn't show any long-term trends and it is mostly variable by ±2 hPa. The global mean O_3 at 1 hPa shows the slight increasing tendency signifying the recovery phase for a couple of years at the beginning of observations; however, it decreases from 2001 until 2003 and then increases to remain consistent after 2005 until the end of observations with equinoctial maxima and solstitial minima (semi-annual variation). The global CO_2 shows the increasing trend throughout the observations with minima during summer (annual cycle).

The correlation coefficients (r) among the MLR predictors are given in Table 1. The r values less than 0.05 are almost equivalent to zero. Further the r values signifies that the predictors are nearly independent as there is no strong correlation (above ~0.5) observed between any of the two predictors. However, for further evaluation of the minor to moderate correlations between $F_{10.7}$ and O_3 (−0.25), and $F_{10.7}$ and CO_2 (−0.47), the variance inflation factor (VIF) has been calculated among the predictors to diagnose the degree of multicollinearity in the MLR analysis (e.g., Miles, 2014; O'brien, 2007; Ramesh et al., 2020a). It is calculated for the nth predictor as $VIF_n = 1/\left(1 - R_n^2\right)$ with R_n as the coefficient of determination. For $VIF_n \simeq 1$, the predictors are not correlated, and multicollinearity does not exist in the regression model. They are moderately correlated for $1 < VIF_n < 5$. As a rule of thumb, multicollinearity is a cause of concern when $VIF_n > 10$ (e.g., Kutner et al., 2004). Here the VIF values are found to be 1.37, 1.02, 1.02, 1.03, 1.06, 1.11, 1.33 for $F_{10.7}$, QBO10, QBO30, NINO 3.4, NAO, O_3, CO_2 respectively. As the obtained VIF value for each regressor is much less than 10, the results of MLR analysis are believed to be more reliable.

3.5. Zonal Wind Response to the Climate Forcings

The MLR analysis defined in Section 2 has been applied to the monthly mean zonal wind anomalies (ΔU) at each altitude. The wind and predictor anomalies are calculated with respect to the first 5 years of the observations.
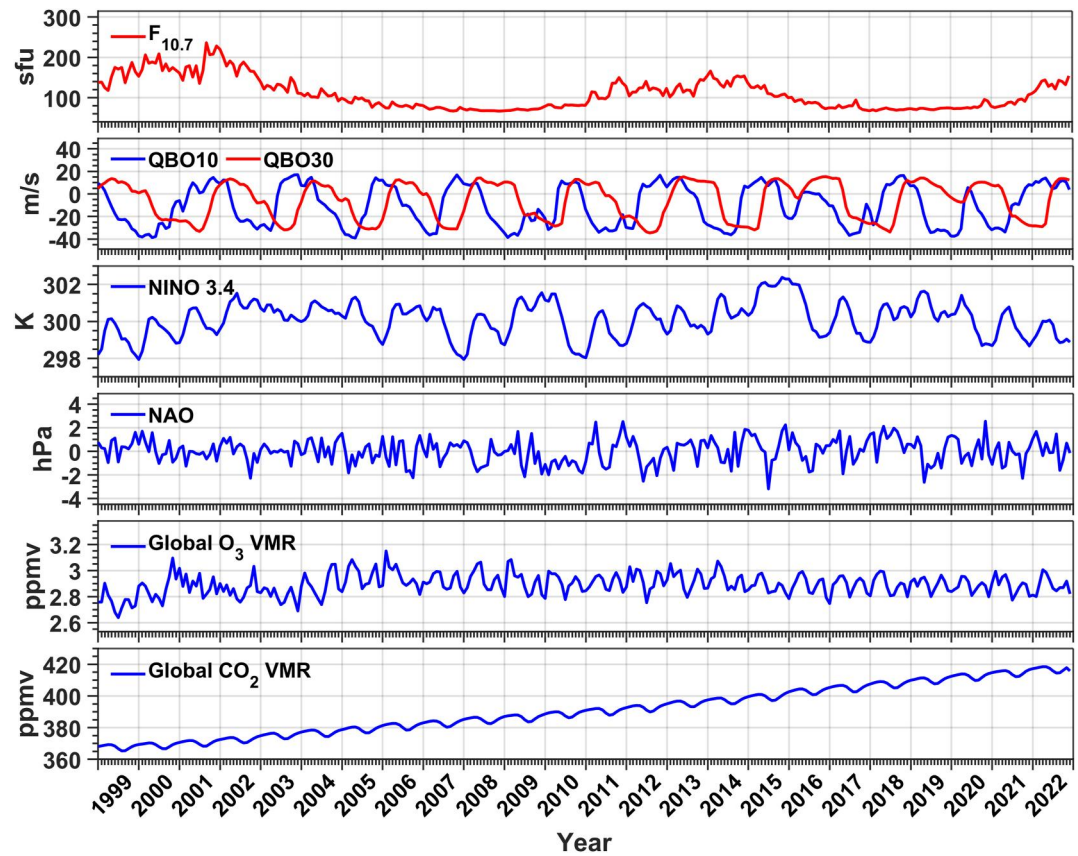
Figure 6. The time series of monthly mean regression indices viz., $F_{10.7}$, QBO10, QBO30, NINO 3.4, North Atlantic Oscillation, O_3, CO_2 for 1999–2022.

Figure 7 illustrates the monthly mean zonal wind anomalies along with their responses to the seven predictors viz., solar ($F_{10.7}$), QBO10, QBO30, NINO 3.4 (ENSO), NAO, O_3, and CO_2. The statistical significance is calculated from t-test (e.g., Wilks, 2006) and the regions where the responses are significant at 90% confidence level are indicated by stippling in the figure. As seen in the figure, the solar response is positive and significant at ~93–99 km during January-February and at around 83–88 km during August-September. However, it is significantly negative at ~88–98 km during September-October and at around ~80 km through July-August. The positive responses denote the enhanced eastward winds are likely due to the solar maximum in winter/spring and the negative responses correspond to weakening/reversal of eastward winds leading to strengthening of the westward winds in summer and autumnal equinox. It can be noted that the zonal wind response to solar activity is not uniform but varies with height and month/season. For example, the enhanced incoming solar radiation during

Table 1
Correlation Coefficients Among the Regressors

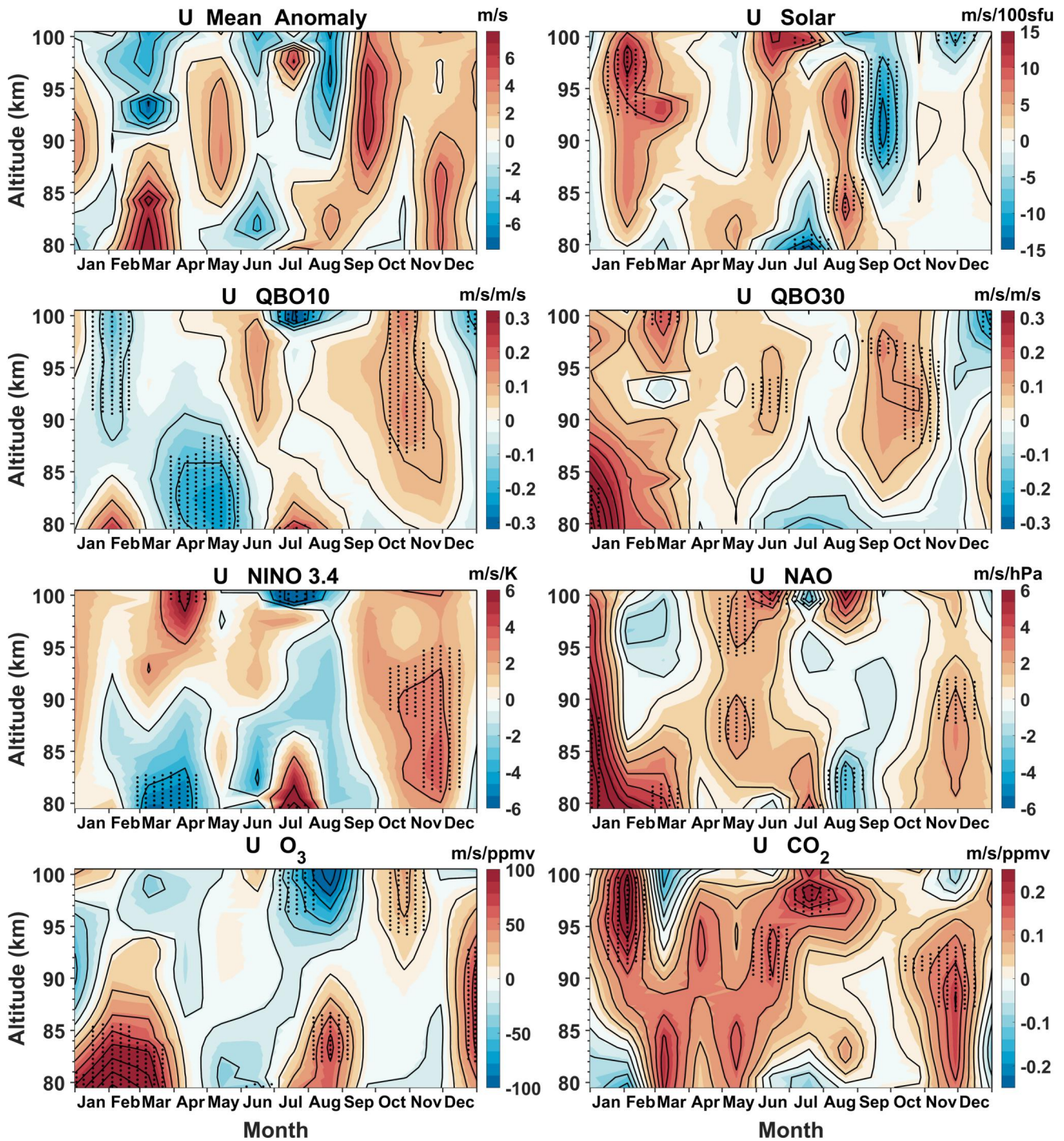|	$F_{10.7}$	QBO10	QBO30	NINO 3.4	NAO	O_3	CO_2
$F_{10.7}$	1.0000						
QBO10	0.0413	1.0000					
QBO30	−0.0635	−0.0903	1.0000				
NINO 3.4	−0.0745	−0.0808	6.5268e−04	1.0000			
NAO	0.1016	−0.0240	−0.0075	−0.1105	1.0000		
O_3	−0.2508	−0.0341	−0.0521	0.1328	−0.1818	1.0000	
CO_2	−0.4744	0.0501	0.0728	0.0798	0.0634	0.1450	1.0000

Figure 7. Monthly mean zonal wind anomalies along with their responses to the seven predictors viz., solar ($F_{10.7}$), QBO10, QBO30, NINO 3.4 (El Niño-Southern Oscillation), North Atlantic Oscillation, O_3 and CO_2 in the mesosphere and lower thermosphere region (~80–100 km) over Esrange.

solar maximum tend to enhance the eastward winds above summer westward winds over ~97 km. The QBO at 10 and 30 hPa are responding to the zonal wind in opposite manner especially in winter and spring equinox. The response due to QBO10 is negative and significant above ~90 km in January-February and below this height during April-May. The QBO30 response is positive in winter but significant only in January at ~80–85 km with relatively strong eastward flow and above ~98 km in March. However, both QBO10 and QBO30 show the significant negative response above ~98 km in December. In addition, the response due to both the indices is

significantly positive above ~88 km in October-November strengthening the climatological eastward flow during autumnal equinox.

The NINO 3.4 index, a proxy for ENSO, comprises El Niño or La Niña events that are defined when the NINO 3.4 SST anomalies respectively exceed +0.4 or −0.4°C for a period of 6 months or more (https://climatedataguide. ucar.edu/climate-data/nino-sst-indices-nino-12-3-34-4-oni-and-tni). As seen in Figure 7, the response of zonal winds to ENSO is not consistent at all the heights/months. It is positive and significantly stronger at around ~82–95 km during the late autumn/early winter (October-December) when the El Niño reaches to peak intensity. It signifies that the eastward winds are intensified due to the El Niño during autumn and winter. The ENSO response is negative and significantly stronger at ~80–83 km in the early spring (March-April) when the El Niño/La Niña tend to develop to reverse the eastward winds to westward, however the response is positive to strengthen the eastward winds above 95 km. Further the response due to ENSO is positive to reverse the summer westward winds below ~83–85 km and it is negative reversing the westerlies above ~98 km which is more pronounced in the month of July. The NAO is deemed to be competent in affecting the northern hemispheric (NH) mean circulation especially over the Atlantic and European regions. As illustrated in Figure 7, the NAO response is positive from late autumn to winter, but stronger at all heights in January and significant only up to ~88 km in part of the month. Further it persists into the early spring below ~85–87 km with significant response up to ~83 km in March. The significant positive response can also be noticed in the late spring at ~86–90 and ~95–100 km. In late summer and early autumn, the response due to NAO reverses to negative which is mostly insignificant except in August at ~82–84 km.

The O_3, that plays crucial role for the polar middle atmosphere dynamics, has greater impact on eastward winds in winter and early spring (Figure 7). Its strong positive response likely to amplify the eastward winds during December-March, however it is not consistent at all observational heights. The significant responses are limited to ~83–94 km in December whereas they are up to ~85 km during January-March. In summer, the impact of O_3 on the MLT zonal winds varies with height. Its response is significantly positive in late summer to reverse the westward winds to eastward below ~90 km, while it is negative above this height reversing the eastward winds to westward. Another significant region of positive response can be found during late autumnal equinox to strengthen the eastward winds above ~95 km. As being another potential constituent to influence the middle atmospheric processes, the significant positive response due to CO_2 denotes the strengthening of eastward winds above ~92 km in the late winter and at ~88–94 km in the late autumn and early winter. The significant positive responses are also observed in summer, but at limited height regions of ~90–95 km in June and above this height in July-August.

3.6. Meridional Wind Response to the Climate Forcings

The monthly mean meridional wind anomalies (ΔV) along with the responses due to the seven predictors are given in Figure 8. The stippled regions in the figure panels represent the significant responses at 90% confidence level. As shown in the figure, the solar response to the meridional winds is negative and significant in the late summer strengthening the equatorward flow during solar maximum; however, the significant regions are limited up to ~88 km and at ~92–97 km, persisting in the early autumn at lower heights. In late autumn and early winter, the solar influence on meridional winds is significantly positive, likely to reverse the equatorward winds to poleward strengthening at ~82–92 km. The QBO10 response is significantly positive, amplifying the poleward winds up to ~87 km in the late winter/early spring, and above ~96 km in summer and early autumn. The response due to QBO30 is significantly positive above ~86 km in late summer and late autumnal equinox, and below ~85 km in early winter, likely to reverse the equatorward winds to poleward. However, it is significantly negative above ~90 km to intensify the equatorward flow in January. The regions of significantly negative responses can also be observed up to ~90 km in July-August and at ~86–93 km during March-April.

The response of ENSO is negative in summer and early autumn, but significantly larger in July and in September up to ~87 and ~90 km respectively, indicating to strengthen the equatorward flow. The regions of significantly negative response can also be seen in the month of October at ~96–98 km. The significant positive responses of ΔV to ENSO are evidenced below ~83 km in November-December likely to amplify the poleward flow, and above ~97 km in December to reverse the equatorward flow. The strong positive response above ~84 km during May-July, peaking at ~95–98 km, denotes the reversal of equatorward flow and strengthening of the poleward flow possibly associated with El Niño; however, it is statistically insignificant. As an important driver of the
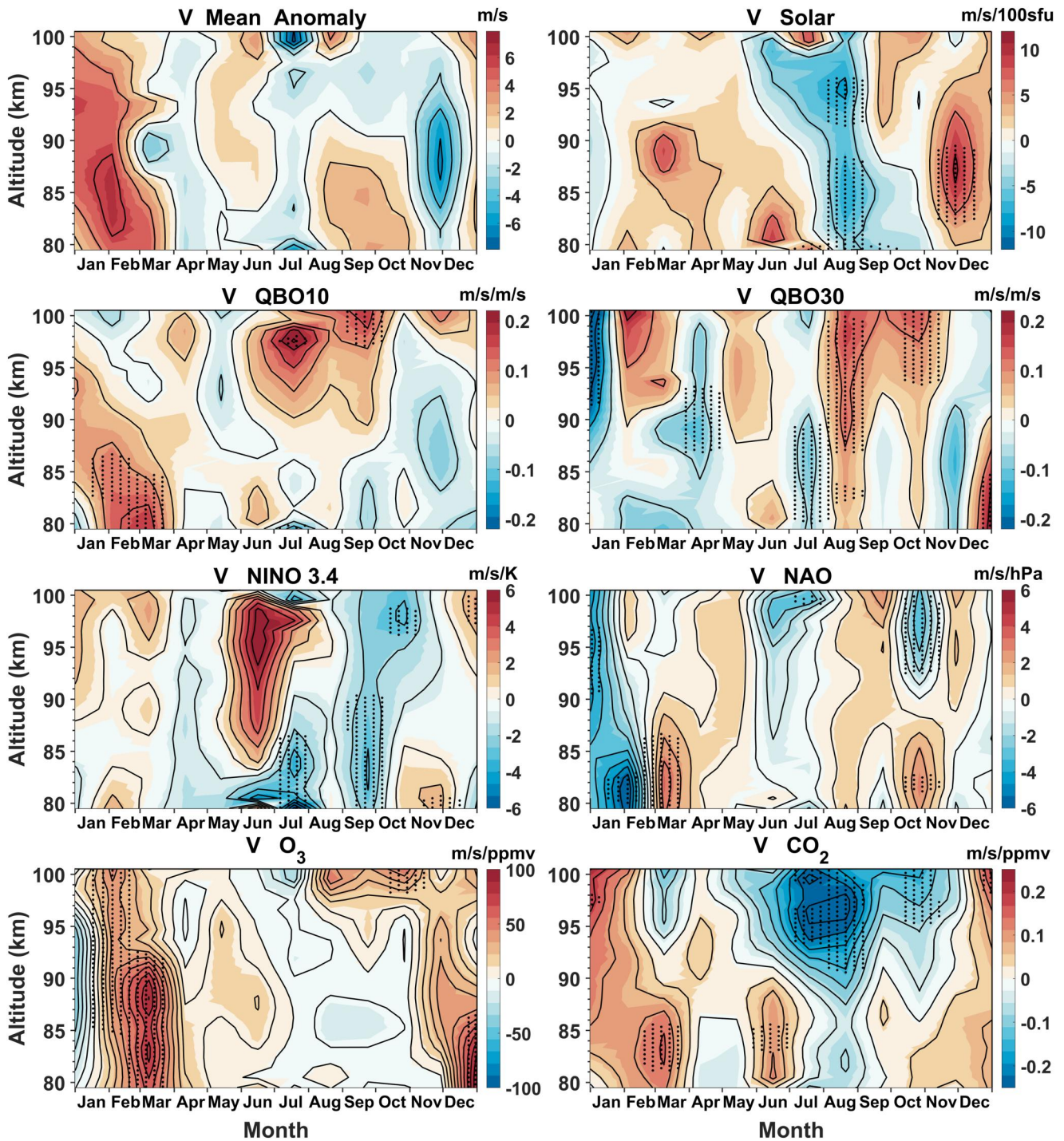
Figure 8. Same as Figure 7 but for meridional winds.

regional climate variability, the NAO exhibits significant impact on meridional winds in winter with strong negative response in January-February below ~84 km and at ~92–97 km likely to strengthen the equatorward winds. In the early spring (March), the response is significantly positive below ~87 km to amplify the poleward winds. In the late autumn, the effect of NAO is likely to intensify the poleward winds below ~85 km and equatorward winds above ~90 km during October-November by the corresponding positive and negative responses of ΔV.
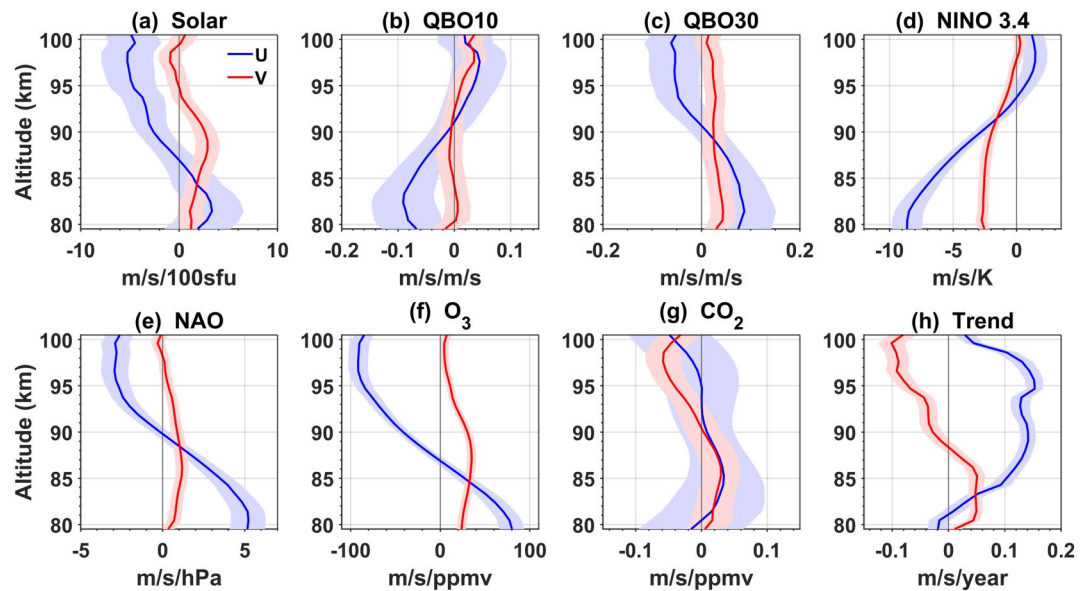
Figure 9. Vertical profiles of cumulative zonal (in blue) and meridional (in red) wind (a–g) responses to the seven predictors, and (h) trends. The blue and red patches in each panel denote the corresponding standard errors.

The response of meridional winds to O_3 is significantly positive strengthening the poleward flow in the late winter and early spring. Further the regions of significant positive responses can be found in the early winter (December) below ∼88 km likely to reverse the equatorward winds to poleward. In summer and autumn, the responses are insignificant except during October-November above ∼97 km. The CO_2 influence is more pronounced in summer with significantly large negative response above ∼90 km to strengthen the equatorward winds. However, below this height, the response is positive in June likely to weaken and reverse the equatorward jet to poleward. Further the significant positive response can be found in the late winter/early spring at ∼82–86 km, also in December-January at the higher altitudes of the observations. The significant negative response above ∼95 km in the late autumn denotes the strengthening of the equatorward winds possibly due to CO_2.

3.7. Aggregate Responses of the Zonal and Meridional Winds to the Climate Forcings

The ΔU and ΔV responses to the seven climate forcings viz., solar activity, QBO10, QBO30, ENSO, NAO, O_3, and CO_2 for all the months and years during 1999–2022 in the MLT region between ∼80 and ∼100 km are computed from MLR analysis. Figures 9a–9g illustrates the altitude variation of cumulative (long-term) responses of the arctic MLT winds to the seven potential drivers. The zonal wind response to SC is positive up to ∼88 km and above this height, it reverses to negative and increases with height. The meridional wind response is positive and slightly increases with height above ∼80 km and decreases from ∼88 km, reverses to negative above ∼95 km. The response of zonal wind to QBO10 is negative below ∼90 km (peaking at ∼83 km) and it reverses to positive above this height. The response of zonal winds to QBO30 is opposite to that of QBO10. It is positive below ∼90 km and negative above this height. The response of meridional wind to QBO10 is insignificant (i.e., falls within the uncertainty limits indicated by the shaded area in the figure) up to ∼97 km and positive above this height, while it is consistently positive for the QBO30.

The zonal wind response to ENSO (NINO 3.4 index) is negative and maximum at lowermost heights; however, it decreases with height and reverses to positive above ∼93 km. The meridional wind response is negative and decreases with height, turns to positive at higher altitudes (above ∼98 km). The zonal wind response to NAO is positive and maximum at lowermost heights and decreases with height, reverses to negative above ∼90 km. The meridional wind response to NAO is positive and slightly increases up to ∼87 km, and it decreases above this height and becomes negative beyond ∼98 km which is not significant. The zonal wind response to O_3 is like that of NAO. It is positive and maximum at lowermost heights, decreases with height and reverses to negative above ∼87 km. The response of meridional flow to O_3 is positive and slightly increases with height, peaking at around
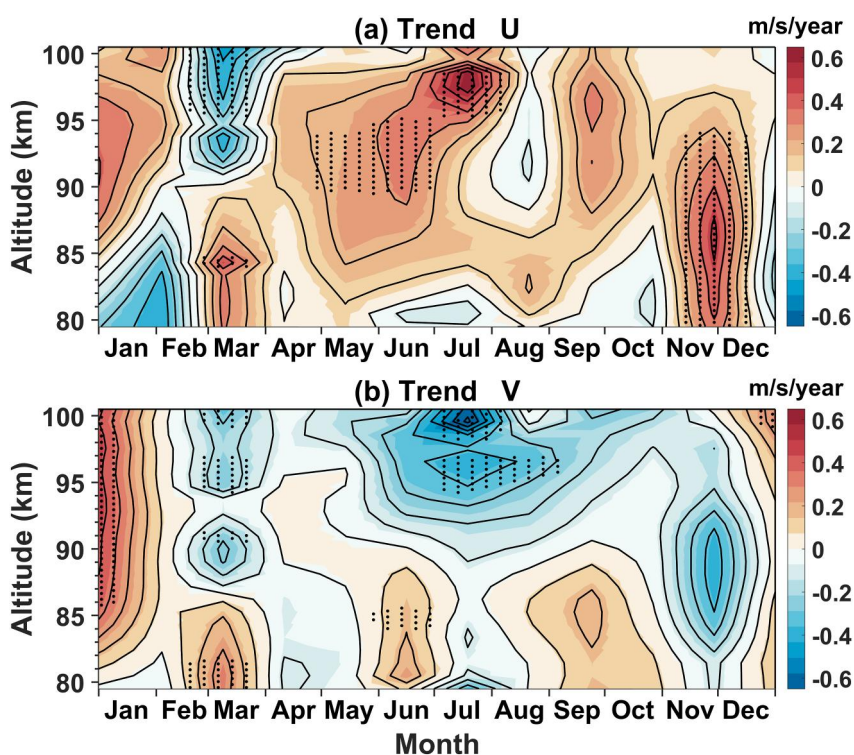
Figure 10. Monthly trends of the (a) zonal, and (b) meridional winds in the mesosphere and lower thermosphere region (∼80–100 km) during the observational period (1999–2022) over Esrange.

∼88 km and decreases above this height. The zonal wind response to CO_2 is insignificant at all heights; however, the meridional wind response is positive below ∼90 km and negative above this height. It increases with height peaking at ∼98 km and decreases above this height.

Furthermore, it can be seen from Figure 9 that the large variabilities in long-term responses are more prominent in zonal winds than meridional winds. Besides, the magnitudes of significant variabilities of the wind responses are larger for O_3 when compared to CO_2.

3.8. Trends in Zonal and Meridional Winds

The cumulative long-term trends ("Trend" signifies changes on a time scale longer than a SC; Ramesh et al., 2020a) in zonal and meridional winds are shown in Figure 9h. Here the trends represent the rate of change of ΔU and ΔV (per year) for all the months and years during the observational period. They are calculated irrespective of climate forcings with no trend (time) term included in the MLR analysis (Equation 1) as there exits strong correlation between the CO_2 and trend (time). The trend in zonal wind is positive and increases above ∼82 km with maximum at ∼95 km (∼0.15 ± 0.01 m/s/year), representing the increasing trend in eastward winds; however, it decreases above this height. The trend in meridional wind is consistently positive at ∼81–85 km and decreases above this height and turns to negative above ∼88 km. The negative trend in meridional wind increases with height and peaks at higher altitudes (−0.1 ± 0.02 m/s/year at ∼99.5 km), indicating the decreasing and increasing trends in poleward and equatorward winds respectively.

The monthly trends in zonal and meridional wind anomalies (with respect to 1999–2003) are calculated for the period 1999–2022 and shown in Figures 10a and 10b. The stippled regions in the figure panels represent the significant trends at 90% confidence level. Here the monthly trends represent the rate of change of ΔU and ΔV (per year) for each month during the observational period. They are calculated regardless of climate forcings with no trend (time) term included in the MLR analysis (Equation 1) due to large correlation between the CO_2 and trend (time). The trends in zonal winds (Figure 10a) are positive and significantly larger in late autumn and early

winter (November-December) up to ~95 km peaking (~0.6 m/s/year) at ~85–88 km, implying an increasing trend of eastward winds. Further the significant positive trend at ~90–95 km in late spring and early summer (May-June), and the strong positive trend (~0.6 m/s/year) above this height in late summer (July-August) indicates the increasing trend of the eastward flow. In the early spring (March), the trends in zonal winds are positive up to ~88–90 km and negative above this height denotes the increasing and decreasing trend in the eastward winds respectively. The trends in meridional winds (Figure 10b) are negative and significantly larger above ~95 km in the late summer (July-August) peaking at ~98–100 km (up to −0.6 m/s) indicates the increasing trends of equatorward winds. The significant negative trends can also be observed during February-March above ~88 km. However, below this height, the significant positive trends imply the increasing trend of poleward winds. The positive trends observed at around ~85 km in June, and above this height in January represent the decreasing trend of equatorward winds.

4. Summary and Discussion

The present study investigates the long-term tendencies and interannual variabilities of polar MLT zonal and meridional winds using meteor radar observations at ~80–100 km during 1999–2022 over Esrange (67.9°N, 21.1°E). In addition, for the first time, the influence of significant drivers viz., solar activity, QBO at 10 and 30 hPa, ENSO, NAO, O_3, and CO_2 on the change in monthly zonal and meridional winds from 1999 to 2003 has been investigated using MLR analysis. The findings are of great importance for comprehensive understanding of the impact of solar and potential climate forcings on the wind anomalies and mean circulations in the polar MLT region. There are comparatively few studies of polar MLT wind climatologies for one SC or more in observational length. The present results demonstrate that the seasonal variation of winds reported in shorter duration studies, from Mitchell et al. (2002) onwards appears representative of the long-term behavior. Note that there may be significant differences (biases) between the wind climatologies from the meteor radar observations in this study and those derived from the MF radar measurements (e.g., Manson et al., 2004; Iimura et al., 2011). These biases are recognized by the experimental community and usually lead to an under-estimation of wind speeds by the MF-radar technique and have been attributed to factors that include, (a) scatter from off the beam axis, (b) side-lobe contamination and (c) the need to correct for refractive effects on the beam pointing (e.g., Wilhelm et al., 2017).

The polar MLT zonal winds are characterized by the summer westward flow up to ~90 km and eastward flow above this height. The MLT dynamics is largely governed by the interaction from GWs, PWs and tides. In summer, as the zonal flow is westward in the stratosphere and mesosphere, the GWs with westward phase speed are filtered out and only those waves with eastward phase speed propagate to the higher altitudes in the MLT, and deposit energy and momentum when they break and decelerates the mean flow that causes the wind reversal from westward to eastward above ~90 km. In the winter, the zonal flow is eastward at all heights with the wind speeds of ~10 m/s; however, the eastward flow can reach up to ~25 m/s below ~85 km in late winter during the SSW episodes (based on major or moderate), for example, 2002, 2004, 2006, 2009, 2013, 2019, and 2020 (Figure 2). The effect of SSWs can extend up to the MLT region through vertical coupling and the wind anomalies associated with the stratospheric polar vortex can reach as high as above ~90 km (e.g., Lukianova et al., 2018). The meridional winds exhibit strong summer equatorward jet centered at the mesopause region of ~85–90 km in June-July at the same time when the strong zonal wind shear exists, and the maximum of meridional flow occurs near to the zero-wind line in the zonal wind as reported by the previous investigations (e.g., Manson et al., 2004; Mitchell et al., 2002; Lukianova et al., 2018). Since the zonal winds act as a filter to upward propagating GWs, the momentum drag associated with GW breaking in the mesosphere is eastward in summer and westward in winter. The zonal drag along with the Coriolis force induces a summer-to-winter meridional circulation (e.g., Andrews & McIntyre, 1976; Becker, 2012; Garcia & Solomon, 1985; Holton, 1983; Lindzen, 1981). The most significant feature is that the poleward wind strengthens up to ~15 m/s in the late winter of the SSW years (based on the intensity of the SSW) and extends throughout the altitude range up to ~100 km when compared to minor/non-SSW episodes. The increased poleward winds can be accompanied by the enhanced eastward winds during SSW periods.

The interannual variability in zonal winds varies with height between eastward and westward winds (Figure 4). For example, the variability is more prominent in winter and least for eastward winds in autumn, whereas it is maximum for westward winds in July at ~82.3 km (Figure 5). However, at ~98.3 km, the variability is maximum for eastward winds in August and minimum in May and October. Similarly in the case of meridional winds, the maximum variability occurs in winter and minimum in early summer at lower altitude, while it is larger in almost

all the months but relatively maximum in summer and winter solstices at higher altitude. The interannual variability in polar MLT winds over Esrange can be attributed to the wave activity and other dynamical processes associated with the significant drivers of SC, QBO, ENSO, NAO, O_3, and CO_2 and through thermal wind balance.

Solar activity plays an important role for the thermal and dynamical processes of the polar MLT. Although the zonal winds are associated with temperature gradients, strong dynamical forcings have greater impact on the variability of the MLT winds. In this study, the significant positive response of the zonal winds to 11-year SC variability in later winter (January-February) specifies the intensification of eastward winds associated with enhanced solar flux in solar maximum conditions. Further, the positive response of the meridional flow implies the enhancement of the poleward winds during solar maximum in late autumn and early winter (November-December). Lukianova et al. (2018) reported the enhancement of eastward zonal flow from solar minimum to solar maximum at all heights of the meteor radar observations in the winter MLT over Sodankylä (67.4°N, 26.6°E). They suggested that the stronger eastward winds are accompanied by the strong poleward winds to close the residual circulation, in agreement with the strengthened pole-to-pole mesospheric circulation during solar maximum. The dependence of stratosphere and mesosphere temperature gradients on the solar activity potentially alter the polar MLT winds. The sharpening of the equator to pole temperature gradient in response to enhanced stratospheric ozone chemistry during solar maximum intensifies the mesospheric eastward GW drag which in turn drives a stronger equatorward meridional flow in the summer. Due to solar response, the intensification of summer westward flow at lower heights was also reported by Lukianova et al. (2018). This can be associated with the enhanced westward GW drag at lower heights, and it reverses due to the wave filtering effect and intensifies the eastward flow at higher level during solar maximum conditions. Wilhelm et al. (2019) reported the influence of 11-year SC on the MLT winds from meteor radar observations during 2002–2018 over a high-latitude location, Andenes (69.3°N, 16°E) and the mid-latitude locations of Juliusruh (54.6°N, 13.4°E) and Tavistock (43.3°N, 80.8°W). They found the impact of 11-year oscillation on seasonal basis with high response of zonal winds during summer (around ~80 km) and winter; however, the meridional winds exhibit almost no changes with SC over three locations. In the present study, the wind responses to SC are evidenced in both the components varying with the altitude and month/season.

The QBO10 and QBO30 responses to the zonal flow are positive strengthening the eastward winds in autumn (significant above ~85 km). However, they exhibit opposite responses in mid-winter, negative due to QBO10 (significant above ~85–90 km) and positive due to QBO30 (significant below ~85 km). The manifestation of the stratospheric QBO extends in to the MLT region in both latitude and altitude (e.g., de Wit et al., 2016). The PWs strongly modulate the stratospheric polar vortex in winter and thereby the MLT winds/circulation. Further the PW propagation to the mid- and high-latitudes is essentially influenced by the QBO phase (e.g., Baldwin & Dunkerton, 1998; Holton & Tan, 1980). The regression analysis in the present study shows the significant positive response of zonal winds due to QBO at both pressure levels (10 and 30 hPa) in the late autumn (Figure 7). The PWs can reach the summer polar mesosphere from the opposite winter hemisphere based on the phase of the equatorial mesospheric QBO (e.g., Ford et al., 2009; Hibbins et al., 2009), which is opposite in phase of the stratospheric QBO. When the equatorial QBO is in eastward phase, the mesospheric QBO is westward and PWs are prevented from propagating across the equator, hence the mesospheric vortex is more stable with stronger eastward winds (e.g., Ford et al., 2009). This could be the possible reason for the significant positive responses in the late autumn to strengthen the eastward winds in the MLT in response of the QBO at both pressure levels (Figure 7). Also, in late spring when the westward winds are intensified due to negative response of the QBO10 below ~90 km. However, this is in opposite situation for QBO10 in winter when the PWs interrupt the MLT zonal winds reversing to westwards. The response due to QBO30 in later winter is similar to that in late autumn but more intense below ~90 km. Through Holton-Tan effect (Holton & Tan, 1980), the PWs interrupt the NH polar vortex in winter when the QBO (at 50 hPa) phase is eastwards, resulting in stronger polar vortex. In the westward phase of the QBO, the stratospheric polar vortex is more perturbed by PWs, resulting in weaker vortex. Recently, Pedatella (2023) simulated the influence of stratospheric polar vortex variability on the MLT winds/circulation. He reported that the MLT circulation is influenced strongly due to both strong and weak polar vortices. When the QBO10 phase is eastwards, the polar vortex is stronger and more symmetric and hence the meridional flow is more poleward in late winter and early spring (Figure 8). However, this is observed as converse for QBO30 to strengthen the equatorward winds in January.

The ENSO plays significant role for modulating the stratospheric polar vortex and thereby the MLT winds. The warm phase of ENSO (El Niño) weakens, and the cold phase (La Niña) strengthens the stratospheric polar vortex

through North Pacific teleconnection (e.g., Butler & Polvani, 2011; Camp & Tung, 2007; Domeisen et al., 2019; Garfinkel et al., 2012; Oehrlein et al., 2019; Sassi et al., 2004). As illustrated above, the strong and weak polar vortices in turn could impact the polar MLT wind/circulation patterns. Further the interaction between QBO and ENSO mainly due to strong wave activity during El Niño phase could impact the intensity of the polar vortex (e.g., Hansen et al., 2016 and references therein; V. Kumar et al., 2022 and references therein). The strong positive response of the zonal winds to the ENSO (Figure 7) coincides with that of the QBO10 during autumnal equinox; however, the overlap regions of significant responses can be found between ~85 and ~95 km, also for QBO30 during October-November. Similarly, significant correlations are evidenced for the zonal wind response to ENSO and QBO10 in spring (below ~90 km) and in summer (at lower and higher altitudes). Below ~85–90 km, the meridional winds response to ENSO (Figure 8) illustrates the significantly enhanced equatorward (summer pole to winter pole) residual circulation due to increased eastward GW drag during warm ENSO events. Above this height, due to anomalous GW filtering, the ENSO response of summer meridional flow reverses to poleward, but this is statistically insignificant. It is equatorward at all heights in the autumnal equinox except in November. The tropospheric circulation in the regional scale can be characterized by the NAO over the Atlantic and Europe (Walker & Bliss, 1932). The tropospheric NAO is closely related to the winter stratospheric polar vortex through wave-mean flow interaction (Baldwin et al., 1994; Perlwitz & Graf, 1995), and the MLT winds are significantly modulated by strength of the stratospheric polar vortex. Thus, the variability in polar MLT winds is directly linked to the tropospheric NAO through dynamical coupling. Most of the previous studies neglected the importance of NAO for influencing the polar MLT winds, however the present study incorporated its prominence to investigate the variabilities in polar MLT winds. The zonal wind response to NAO is stronger and positive strengthening the eastward winds in late winter, especially in January (Figure 7). Jacobi and Beckmann (1999) found the strong positive correlation between winter (prominent in January) mesopause eastward winds and the NAO index over Collm observatory (52°N, 15°E), Germany possibly due to dynamical coupling between different layers through PWs. However, they also suggested that the strong correlation cannot be expected in summer as the dynamical coupling between the middle atmosphere and the troposphere is relatively weaker in this season than in winter. In late winter, the significant negative response of the meridional flow (equatorward) to the NAO (Figure 8) is accompanied by the strong positive response (eastward) of the zonal winds (Figure 7).

The response of zonal and meridional winds to ozone in winter and early spring could be the result of interaction of polar vortex to the stratospheric ozone. The response due to ozone significantly intensifies the MLT eastward and poleward winds in the winter and early spring (Figures 7 and 8) by modulating the temperature gradients, winds and thereby the GW filtering effect in the stratosphere. An increase (decrease) in arctic stratospheric ozone corresponds to a weakened (strong) stratospheric polar vortex, which in turn resembles strong (week) Brewer-Dobson circulation (e.g., Hu et al., 2023) based on the PW activity. As the ozone recovery commenced due to declining global ozone depleting substances after 1995 (e.g., Ramesh et al., 2020a), the increasing trend in global ozone (at 1 hPa) appeared at least in the beginning years of the observations (Figure 6). After 2004, the tendency in ozone remains almost consistent with seasonal/interannual variabilities as seen in Figure 6. Here, the enhanced ozone could weaken/reverse the stratospheric eastward flow (due to change in temperature gradients) so that the increased eastward GW drag strengthen the eastward winds in the polar MLT during winter, extended to early spring (Figure 7). This subsequently intensifies the poleward circulation as illustrated in Figure 8. However, the response due to ozone significantly reverses the westward and eastward winds below and above ~90 km respectively, possibly due to the reversal of the GW forcing in the late summer. The increasing CO_2 enhances the tropospheric heating and middle atmosphere radiative cooling. This favors for stronger GW and PW generation in the lower atmosphere and the vertical destabilization impacts the wave propagation into the MLT (e.g., Akmaev & Fomichev, 1998; Rind et al., 1990). The combined stronger momentum deposition by the waves subsequently leads to stronger residual circulation (summer pole to winter pole) in the MLT region (Figure 8). The strong meridional circulation is accompanied by enhanced eastward winds in summer (Figure 7). However, the strong positive response due to CO_2 significantly intensifies the eastward winds in late winter (above ~85–90 km), and this could possibly due to increased eastward GW drag.

The trends in zonal and meridional wind anomalies (change in ΔU and ΔV per year) are calculated from linear least-squares slopes at all observational heights as cumulative (Figure 9h) and for each month (Figure 10) to quantify the long-term changes in arctic MLT winds over Esrange. As CO_2 evolves with time, the strong

correlation between the trend (time) and CO_2 could be a significant concern to interpret the results from regression analysis. Thus, the trend (time) term has been excluded from the MLR (Equation 1) and trends in wind anomalies are estimated regardless the climate forcings. The increasing positive trend in zonal winds signifies the increasing trends of eastward winds above ~82 km (Figure 9h), however it decreases above ~95 km. The trend in meridional wind is positive up to ~88 km and negative above this height. The increasing negative trend in meridional wind represents the decreasing and increasing trends of poleward and equatorward winds respectively. The zonal winds show significant positive trends up to ~95 km in late autumn/early winter and in late spring/summer above ~90 km (Figure 10), representing the increasing trend of eastward winds, can be attributed mainly to the consequences of increasing CO_2 that significantly affect the wave (GW, PW, and tides) generation sources, vertical propagation, and dissipative properties in the polar MLT region. However, the significant negative trend above ~90 km in the late winter/early spring denotes the decreasing trend of eastward winds. The significant negative trend of the meridional winds above ~90–95 km indicates the increasing trend of equatorward winds, possibly due to increasing CO_2 that influence the meridional residual circulation from summer pole to winter pole in the MLT. The significant positive trend in the mid-winter denotes the increasing trend of poleward (northward) winds, possibly due to modulation in the wave activity.

5. Conclusions

The long-term variability and tendencies in polar monthly zonal and meridional winds are derived from the meteor radar observations at ~80–100 km during 1999–2022 (two SCs) over Esrange (67.9°N, 21.1°E). In addition, for the first time, the broad impact of the potential climate forcings viz., SC, QBO (at 10 and 30 hPa), ENSO, NAO, O_3, and CO_2 on the polar MLT winds has been investigated using MLR analysis for the observational period.

The main conclusions of this study can be listed as follows.

i. The zonal winds are characterized by strong easterlies (westward winds) below ~90 km and strong westerlies (eastward winds) above this height in summer (JJA). The meridional flow is characterized by strong equatorward jet centered at ~85–90 km in summer. Although there is a well-defined recurrent seasonal cycle in zonal and meridional winds, there is nevertheless significant inter-annual variability evident in all seasons and at all heights.

ii. The interannual variability in zonal winds is more prominent in winter and summer solstices at lower altitudes (~82.3 km), whereas it is larger in late summer at higher altitudes (~98.5 km). For meridional winds, the large interannual variability occurs in winter and early summer at lower altitudes, while it is considerably larger in all the months, but more pronounced in summer at higher altitudes.

iii. The significant positive responses of zonal and meridional winds to solar activity (up to 15 m/s/100 sfu) in late winter/early spring and in late autumn/early winter respectively indicates the strengthening of eastward and poleward winds during solar maximum conditions.

iv. The responses of zonal and meridional winds to QBO10 and QBO30 are positive in autumnal equinox to strengthen eastward and poleward winds. However, the negative response of zonal wind to QBO10 during late winter/spring denote weakening/reversal of the eastward winds.

v. The response of zonal wind to ENSO is significantly positive and negative to strengthen and weaken the eastward winds in late autumn and spring (below ~90 km) respectively. The response of meridional wind to ENSO is to amplify the equatorward flow in summer (below ~90 km) and early autumn.

vi. The response of zonal wind to NAO is significantly positive in January to intensify the eastward flow, however it is negative for the meridional winds in January-February to weaken/reverse the poleward winds.

vii. The impact of O_3 is significantly strong to strengthen the eastward winds in winter/early spring (below ~90 km) and poleward flow in late winter/early spring.

viii. The CO_2 intensifies the eastward flow in late winter and summer above ~90 km. It amplifies the meridional circulation (summer pole to winter pole) with significant negative response above ~90 km in summer.

ix. For the cumulative trends, the positive trend in zonal wind increases at ~82–95 km and the negative trend in meridional wind increases above ~88 km.

x. The positive trend in zonal wind is significantly larger in summer (above ~90 km) and late autumn/early winter (~0.6 m/s/year). The negative trend in meridional wind is more pronounced in summer above ~95 km (−0.6 m/s/year).

Data Availability Statement

The Esrange meteor radar data can be obtained from the UK Centre for Environmental Data Archival (CEDA) at https://data.ceda.ac.uk/badc/meteor-radars/data/esrange for 2000–2018, and from Genesis software Ltd: https://www.gsoft.com.au/ for the remaining years upon request.

References

Akmaev, R. A., & Fomichev, V. I. (1998). Cooling of the mesosphere and lower thermosphere due to doubling of CO_2. *Annales Geophysicae*, *16*(11), 1501–1512. https://doi.org/10.1007/s00585-998-1501-z

Andrews, D. G., Holton, J. R., & Leovy, C. B. (1987). *Middle atmosphere dynamics*. Academic Press.

Andrews, D. G., & McIntyre, M. E. (1976). Planetary waves in horizontal and vertical shear: The generalized Eliassen-Palm relation and the mean zonal acceleration. *Journal of the Atmospheric Sciences*, *33*(11), 2031–2048. https://doi.org/10.1175/1520-0469(1976)033<2031:PWIHAV>2.0.CO;2

Baldwin, M. P., Cheng, X., & Dunkerton, T. J. (1994). Observed correlations between winter-mean tropospheric and stratospheric circulation anomalies. *Geophysical Research Letters*, *21*(12), 1141–1144. https://doi.org/10.1029/94GL01010

Baldwin, M. P., & Dunkerton, T. J. (1998). Quasi-biennial modulation of the southern hemisphere stratospheric polar vortex. *Geophysical Research Letters*, *25*(17), 3343–3346. https://doi.org/10.1029/98GL02445

Baldwin, M. P., Gray, L. J., Dunkerton, T. J., Hamilton, K., Haynes, P. H., Randel, W. J., et al. (2001). The quasi-biennial oscillation. *Reviews of Geophysics*, *39*(2), 179–229. https://doi.org/10.1029/1999RG000073

Baumgaertner, A. J. G., McDonald, A. J., Fraser, G. J., & Plank, G. E. (2005). Long-term observations of mean winds and tides in the upper mesosphere and lower thermosphere above Scott Base, Antarctica. *Journal of Atmospheric and Solar-Terrestrial Physics*, *67*(16), 1480–1496. https://doi.org/10.1016/j.jastp.2005.07.018

Becker, E. (2012). Dynamical control of the middle atmosphere. *Space Science Reviews*, *168*(1–4), 283–314. https://doi.org/10.1007/s11214-011-9841-5

Bremer, J., Schminder, R., Greisiger, K. M., Hoffmann, P., Kürschner, D., & Singer, W. (1997). Solar cycle dependence and long-term trends in the wind field of the mesosphere/lower thermosphere. *Journal of Atmospheric and Solar-Terrestrial Physics*, *59*(5), 497–509. https://doi.org/10.1016/S1364-6826(96)00032-6

Burrage, M. D., Vincent, R. A., Mayr, H. G., Skinner, W. R., Arnold, N. F., & Hays, P. B. (1996). Long-term variability in the equatorial middle atmosphere zonal wind. *Journal of Geophysical Research*, *101*(D8), 12847–12854. https://doi.org/10.1029/96JD00575

Butler, A. H., & Polvani, L. M. (2011). El Niño, La Niña, and stratospheric sudden warmings: A reevaluation in light of the observational record. *Geophysical Research Letters*, *38*(13), L13807. https://doi.org/10.1029/2011GL048084

Cai, B., Xu, Q. C., Hu, X., Cheng, X., Yang, J. F., & Li, W. (2021). Analysis of the correlation between horizontal wind and 11-year solar activity over Langfang, China. *Earth and Planetary Physics*, *5*(3), 270–279. https://doi.org/10.26464/epp2021029

Camp, C. D., & Tung, K.-K. (2007). Stratospheric polar warming by ENSO in winter: A statistical study. *Geophysical Research Letters*, *34*(4), L04809. https://doi.org/10.1029/2006GL028521

Chau, J. L., Goncharenko, L. P., Fejer, B. G., & Liu, H. L. (2012). Equatorial and low latitude ionospheric effects during sudden stratospheric warming events. *Space Science Reviews*, *168*(1–4), 385–417. https://doi.org/10.1007/s11214-011-9797-5

Cullens, C. Y., England, S. L., & Garcia, R. R. (2016). The 11 year solar cycle signature on wave-driven dynamics in WACCM. *Journal of Geophysical Research: Space Physics*, *121*(4), 3484–3496. https://doi.org/10.1002/2016JA022455

Dawkins, E. C. M., Stober, G., Janches, D., Carrillo-Sánchez, J. D., Lieberman, R. S., Jacobi, C., et al. (2023). Solar cycle and long-term trends in the observed peak of the meteor altitude distributions by meteor radars. *Geophysical Research Letters*, *50*(2), e2022GL101953. https://doi.org/10.1029/2022GL101953

Dempsey, S. M., Hindley, N. P., Moffat-Griffin, T., Wright, C. J., Smith, A. K., Du, J., & Mitchell, N. J. (2021). Winds and tides of the Antarctic mesosphere and lower thermosphere: One year of meteor-radar observations over Rothera (68°S, 68°W) and comparisons with WACCM and eCMAM. *Journal of Atmospheric and Solar-Terrestrial Physics*, *212*, 105510. https://doi.org/10.1016/j.jastp.2020.105510

de Wit, R. J., Janches, D., Fritts, D. C., & Hibbins, R. E. (2016). QBO modulation of the mesopause gravity wave momentum flux over Tierra del Fuego. *Geophysical Research Letters*, *43*(8), 4049–4055. https://doi.org/10.1002/2016GL068599

Domeisen, D. I., Garfinkel, C. I., & Butler, A. H. (2019). The teleconnection of el Niño southern oscillation to the stratosphere. *Reviews of Geophysics*, *57*(1), 5–47. https://doi.org/10.1029/2018RG000596

Dunkerton, T. J., & Baldwin, M. P. (1991). Quasi-biennial modulation of planetary-wave fluxes in the northern hemisphere winter. *Journal of the Atmospheric Sciences*, *48*(8), 1043–1061. https://doi.org/10.1175/1520-0469(1991)048<1043:qbmopw>2.0.co;2

Dutta, R., & Sridharan, S. (2023). Observational evidence for the influence of diurnal tide in driving winds in the polar upper mesosphere and lower thermosphere. *Journal of Geophysical Research: Space Physics*, *128*(3), e2022JA031104. https://doi.org/10.1029/2022JA031104

Emmert, J., Stevens, M., Bernath, P., Drob, D. P., & Boone, C. D. (2012). Observations of increasing carbon dioxide concentration in Earth's thermosphere. *Nature Geoscience*, *5*(12), 868–871. https://doi.org/10.1038/ngeo1626

Ford, E. A. K., Hibbins, R. E., & Jarvis, M. J. (2009). QBO effects on Antarctic mesospheric winds and polar vortex dynamics. *Geophysical Research Letters*, *36*(20), L20801. https://doi.org/10.1029/2009GL039848

Fritts, D. C., & Alexander, M. J. (2003). Gravity wave dynamics and effects in the middle atmosphere. *Reviews of Geophysics*, *41*, 1003. https://doi.org/10.1029/2001RG000106

Garcia, R. R., López-Puertas, M., Funke, B., Marsh, D. R., Kinnison, D. E., Smith, A. K., & González-Galindo, F. (2014). On the distribution of CO_2 and CO in the mesosphere and lower thermosphere. *Journal of Geophysical Research: Atmospheres*, *119*(9), 5700–5718. https://doi.org/10.1002/2013JD021208

Garcia, R. R., & Solomon, S. (1985). The effect of breaking gravity waves on the dynamics and chemical composition of the mesosphere and lower thermosphere. *Journal of Geophysical Research*, *90*(D2), 3850–3868. https://doi.org/10.1029/JD090iD02p03850

Garfinkel, C. I., Butler, A. H., Waugh, D. W., Hurwitz, M. M., & Polvani, L. M. (2012). Why might stratospheric sudden warmings occur with similar frequency in El Niño and La Niña winters? *Journal of Geophysical Research*, *117*(D19), D19106. https://doi.org/10.1029/2012JD017777

Greisiger, K. M., Schminder, R., & KuÈrschner, D. (1987). Long-period variations of wind parameters in the mesopause region and the solar cycle dependence. *Journal of Atmospheric and Terrestrial Physics*, *49*(3), 281–285. https://doi.org/10.1016/0021-9169(87)90063-8

Gurubaran, S., Dhanya, R., Sathishkumar, S., & Paramasivan, B. (2007). On the electric field control of the MF radar scatterers in the lower E region over the magnetic equator. *Geophysical Research Letters*, *34*(6), L06105. https://doi.org/10.1029/2006GL028748

Gurubaran, S., & Rajaram, R. (1999). Long-term variability in the mesospheric tidal winds observed by MF radar over Tirunelveli (8.7°N, 77.8° E). *Geophysical Research Letters*, *26*(8), 1113–1116. https://doi.org/10.1029/1999GL900171

Gurubaran, S., Rajaram, R., Nakamura, T., & Tsuda, T. (2005). Interannual variability of diurnal tide in the tropical mesopause region: A signature of the el Nino-southern oscillation (ENSO). *Geophysical Research Letters*, *32*(13), L13805. https://doi.org/10.1029/2005GL022928

Hall, C. M., Aso, T., Tsutsumi, M., Nozawa, S., Manson, A. H., & Meek, C. E. (2005). A comparison of mesosphere and lower thermosphere neutral winds as determined by meteor and medium-frequency radar at 70°N. *Radio Science*, *40*(4), RS4001. https://doi.org/10.1029/2004RS003102

Hansen, F., Matthes, K., & Wahl, S. (2016). Tropospheric QBO–ENSO interactions and differences between the Atlantic and Pacific. *Journal of Climate*, *29*(4), 1353–1368. https://doi.org/10.1175/JCLI-D-15-0164.1

Haurwitz, B. (1961). Frictional effects and the meridional circulation in the mesosphere. *Journal of Geophysical Research*, *66*(8), 2381–2391. https://doi.org/10.1029/JZ066i008p02381

Hibbins, R. E., Espy, P. J., & Jarvis, M. J. (2007). Quasi-biennial modulation of the semidiurnal tide in the upper mesosphere above Halley, Antarctica. *Geophysical Research Letters*, *34*(21), L21804. https://doi.org/10.1029/2007GL031282

Hibbins, R. E., Jarvis, M. J., & Ford, E. A. K. (2009). Quasi-biennial oscillation influence on long-period planetary waves in the Antarctic upper mesosphere. *Journal of Geophysical Research*, *114*(D9), D09109. https://doi.org/10.1029/2008JD011174

Hindley, N. P., Mitchell, N. J., Cobbett, N., Smith, A. K., Fritts, D. C., Janches, D., et al. (2022). Radar observations of winds, waves and tides in the mesosphere and lower thermosphere over South Georgia island (54°S, 36°W) and comparison with WACCM simulations. *Atmospheric Chemistry and Physics*, *22*(14), 9435–9459. https://doi.org/10.5194/acp-22-9435-2022

Hocking, W. K., Fuller, B., & Vandepeer, B. (2001). Real-time determination of meteor-related parameters utilizing modern digital technology. *Journal of Atmospheric and Solar-Terrestrial Physics*, *63*(2–3), 155–169. https://doi.org/10.1016/S1364-6826(00)00138-3

Hoffmann, P., Singer, W., Keuer, D., Hocking, W. K., Kunze, M. K., & Murayama, Y. (2007). Latitudinal and longitudinal variability of mesospheric winds and temperature during stratospheric warming events. *Journal of Atmospheric and Solar-Terrestrial Physics*, *69*(17–18), 2355–2366. https://doi.org/10.1016/j.jastp.2007.06.010

Holton, J. R. (1982). The role of gravity wave induced drag and diffusion in the momentum budget of the mesosphere. *Journal of the Atmospheric Sciences*, *39*(4), 791–799. https://doi.org/10.1175/1520-0469(1982)039<0791:TROGWI>2.0.CO;2

Holton, J. R. (1983). The dynamics of large scale atmospheric motions. *Reviews of Geophysics*, *21*(5), 1021–1027. https://doi.org/10.1029/RG021i005p01021

Holton, J. R., & Tan, H. (1980). The influence of the equatorial quasi-biennial oscillation on the global circulation at 50 mb. *Journal of the Atmospheric Sciences*, *37*(10), 2200–2208. https://doi.org/10.1175/1520-0469(1980)037<2200:TIOTEQ>2.0.CO;2

Hu, D., Shi, S., & Wang, Z. (2023). Link between Arctic ozone and the stratospheric polar vortex. *Atmospheric and Oceanic Science Letters*, *16*(1), 1–6. https://doi.org/10.1016/j.aosl.2022.100293

Iimura, H., Fritts, D. C., Tsutsumi, M., Nakamura, T., Hoffmann, P., & Singer, W. (2011). Long-term observations of the wind field in the Antarctic and Arctic mesosphere and lower-thermosphere at conjugate latitudes. *Journal of Geophysical Research*, *116*(D20), D20112. https://doi.org/10.1029/2011JD016003

Jackson, D. R., Fuller-Rowell, T. J., Griffin, D. J., Griffith, M. J., Kelly, C. W., Marsh, D. R., & Walach, M.-T. (2019). Future directions for whole atmosphere modeling: Developments in the context of space weather. *Space Weather*, *17*(9), 1342–1350. https://doi.org/10.1029/2019SW002267

Jacobi, C. (2012). 6 year mean prevailing winds and tides measured by VHF meteor radar over Collm (51.3°N, 13.0°E). *Journal of Atmospheric and Solar-Terrestrial Physics*, *78–79*, 8–18. https://doi.org/10.1016/j.jastp.2011.04.010

Jacobi, C., & Beckmann, B. R. (1999). On the connection between upper atmospheric dynamics and tropospheric parameters: Correlations between mesopause region winds and the North Atlantic oscillation. *Climatic Change*, *43*(3), 629–643. https://doi.org/10.1023/A:1005451227975

Jacobi, C., Hoffmann, P., Liu, R. Q., Merzlyakov, E. G., Portnyagin, Y. I., Manson, A. H., & Meek, C. E. (2012). Long-term trends, their changes, and interannual variability of Northern Hemisphere midlatitude MLT winds. *Journal of Atmospheric and Solar-Terrestrial Physics*, *75–76*, 81–91. https://doi.org/10.1016/j.jastp.2011.03.016

Jacobi, C., Lilienthal, F., Geißler, C., & Krug, A. (2015). Long-term variability of mid-latitude mesosphere-lower thermosphere winds over Collm (51°N, 13°E). *Journal of Atmospheric and Solar-Terrestrial Physics*, *136*, 174–186. https://doi.org/10.1016/j.jastp.2015.05.006

Jacobi, C., Portnyagin, Y. I., Merzlyakov, E. G., Solovjova, T. V., Makarov, N. A., & Kürschner, D. (2005). A long-term comparison of mesopause region wind measurements over Eastern and Central Europe. *Journal of Atmospheric and Solar-Terrestrial Physics*, *67*(3), 229–240. https://doi.org/10.1016/j.jastp.2004.10.002

Jacobi, C., Schminder, R., & Kürschner, D. (1996). On the influence of the stratospheric quasi-biennial oscillation on the mesopause zonal wind over central Europe. *Meteorologische Zeitschrift*, *5*(6), 318–323. https://doi.org/10.1127/metz/5/1996/318

Jaen, J., Renkwitz, T., Liu, H., Jacobi, C., Wing, R., Kuchař, A., et al. (2023). Long-term studies of the summer wind in the mesosphere and lower thermosphere at middle and high latitudes over Europe. *Atmospheric Chemistry and Physics*, *23*, 14871–14887. https://doi.org/10.5194/acp-23-14871-2023

Kishore Kumar, G., Kishore Kumar, K., Singer, W., Zülicke, C., Gurubaran, S., Baumgarten, G., et al. (2014). Mesosphere and lower thermosphere zonal wind variations over low latitudes: Relation to local stratospheric zonal winds and global circulation anomalies. *Journal of Geophysical Research: Atmospheres*, *119*(10), 5913–5927. https://doi.org/10.1002/2014JD021610

Kolstad, E. W., Wulff, C. O., Domeisen, D. I. V., & Woollings, T. (2020). Tracing North Atlantic oscillation Forecast errors to stratospheric origins. *Journal of Climate*, *33*(21), 9145–9157. https://doi.org/10.1175/JCLI-D-20-0270.1

Kumar, K. K., Deepa, V., Antonita, M., & Ramkumar, G. (2008). Meteor radar observations of short-term tidal variabilities in the low-latitude mesosphere-lower thermosphere: Evidence for nonlinear wave-wave interactions. *Journal of Geophysical Research*, *113*(D16), D16108. https://doi.org/10.1029/2007JD009610

Kumar, K. K., Ramkumar, G., & Shelbi, S. T. (2007). Initial results from SKiYMET meteor radar at Thumba (8.5°N, 77°E): 1. Comparison of wind measurements with MF spaced antenna radar system. *Radio Science*, *42*(6), RS6008. https://doi.org/10.1029/2006RS003551

Kumar, V., Yoden, S., & Hitchman, M. H. (2022). QBO and ENSO effects on the mean meridional circulation, polar vortex, subtropical westerly jets, and wave patterns during boreal winter. *Journal of Geophysical Research: Atmospheres*, *127*(15), e2022JD036691. https://doi.org/10.1029/2022JD036691

Kutner, M. H., Nachtsheim, C. J., & Neter, J. (2004). *Applied linear regression models* (4th ed.). McGraw-Hill Irwin.

Laštovička, J., Akmaev, R. A., Beig, G., Bremer, J., Emmert, J. T., Jacobi, C., et al. (2008). Emerging pattern of global change in the upper atmosphere and ionosphere. *Annales Geophysicae*, *26*(5), 1255–1268. https://doi.org/10.5194/angeo-26-1255-2008

Lieberman, R. S., Riggin, D. M., Ortland, D. A., Nesbitt, S. W., & Vincent, R. A. (2007). Variability of mesospheric diurnal tides and tropospheric diurnal heating during 1997–1998. *Journal of Geophysical Research*, *112*(D20), D20110. https://doi.org/10.1029/2007JD008578

Lindzen, R. S. (1981). Turbulence and stress owing to gravity wave and tidal breakdown. *Journal of Geophysical Research*, *86*(C10), 9707–9714. https://doi.org/10.1029/JC086iC10p09707

Liu, H., Sun, Y.-Y., Miyoshi, Y., & Jin, H. (2017). ENSO effects on MLT diurnal tides: A 21 year reanalysis data-driven GAIA model simulation. *Journal of Geophysical Research: Space Physics*, *122*(5), 5539–5549. https://doi.org/10.1002/2017JA024011

Liu, X., Xu, J., Yue, J., & Andrioli, V. F. (2023). Variations in global zonal wind from 18 to 100 km due to solar activity and the quasi-biennial oscillation and El Niño–Southern Oscillation during 2002–2019. *Atmospheric Chemistry and Physics*, *23*(11), 6145–6167. https://doi.org/10.5194/acp-23-6145-2023

Lübken, F.-J., & von Zahn, U. (1991). Thermal structure of the mesopause region at polar latitudes. *Journal of Geophysical Research*, *96*(D11), 20841–20857. https://doi.org/10.1029/91JD02018

Lukianova, R., Kozlovsky, A., & Lester, M. (2018). Climatology and inter-annual variability of the polar mesospheric winds inferred from meteor radar observations over Sodankylä (67N, 26E) during solar cycle 24. *Journal of Atmospheric and Solar-Terrestrial Physics*, *171*, 241–249. https://doi.org/10.1016/j.jastp.2017.06.005

Lukianova, R., Kozlovsky, A., Shalimov, S., Ulich, T., & Lester, M. (2015). Thermal and dynamical perturbations in the winter polar mesosphere-lower thermosphere region associated with sudden stratospheric warmings under conditions of low solar activity. *Journal of Geophysical Research: Space Physics*, *120*(6), 5226–5240. https://doi.org/10.1002/2015JA021269

Manson, A. H., Meek, C. E., Hall, C. M., Nozawa, S., Mitchell, N. J., Pancheva, D., et al. (2004). Mesopause dynamics from the Scandinavian triangle of radars within the PSMOS-DATAR project. *Annales Geophysicae*, *22*(2), 367–386. https://doi.org/10.5194/angeo-22-367-2004

Marsh, D., & Roble, R. (2002). TIME-GCM simulations of lower-thermospheric nitric oxide seen by the halogen occultation experiment. *Journal of Atmospheric and Solar-Terrestrial Physics*, *64*(8–11), 889–895. https://doi.org/10.1016/S1364-6826(02)00044-5

Miles, J. (2014). Tolerance and variance inflation factor. In N. Balakrishnan, T. Colton, B. Everitt, W. Piegorsch, F. Ruggeri, & J. L. Teugels (Eds.), *Wiley StatsRef: Statistics reference online*. John Wiley & Sons, Ltd. https://doi.org/10.1002/9781118445112.stat06593

Mitchell, N. J., Pancheva, D., Middleton, H. R., & Hagan, M. (2002). Mean winds and tides in the Arctic mesosphere and lower thermosphere. *Journal of Geophysical Research*, *107*(A1), 1004. https://doi.org/10.1029/2001JA900127

Namboothiri, S. P., Manson, A. H., & Meek, C. E. (1993). Variations of mean winds and tides in the upper middle atmosphere over a solar cycle, Saskatoon, Canada, 52°N, 107°W. *Journal of Atmospheric and Terrestrial Physics*, *55*(10), 1325–1334. https://doi.org/10.1016/0021-9169(93)90101-4

Namboothiri, S. P., Meek, C. E., & Manson, A. H. (1994). Variations of mean winds and solar tides in the mesosphere and lower thermosphere over time scales ranging from 6 months to 11 yr: Saskatoon, 52°N, 107°W. *Journal of Atmospheric and Terrestrial Physics*, *56*(10), 1313–1325. https://doi.org/10.1016/0021-9169(94)90069-8

O'brien, R. M. (2007). A caution regarding rules of thumb for variance inflation factors. *Quality and Quantity*, *41*(5), 673–690. https://doi.org/10.1007/s11135-006-9018-6

Oehrlein, J., Chiodo, G., & Polvani, L. M. (2019). Separating and quantifying the distinct impacts of El Niño and sudden stratospheric warmings on North Atlantic and Eurasian wintertime climate. *Atmospheric Science Letters*, *20*(7), e923. https://doi.org/10.1002/asl.923

Pedatella, N. M. (2023). Influence of stratosphere polar vortex variability on the mesosphere, thermosphere, and ionosphere. *Journal of Geophysical Research: Space Physics*, *128*(7), e2023JA031495. https://doi.org/10.1029/2023JA031495

Perlwitz, J., & Graf, H. F. (1995). The statistical connection between tropospheric and stratospheric circulation of the Northern-Hemisphere in winter. *Journal of Climate*, *8*(10), 2281–2295. https://doi.org/10.1175/1520-0442(1995)008<2281:TSCBTA>2.0.CO;2

Portnyagin, Y. I., Merzlyakov, E. G., Solovjova, T. V., Jacobi, C., Kurschner, D., Manson, A., & Meek, C. (2006). Long-term trends and year-to-year variability of mid-latitude mesosphere/lower thermosphere winds. *Journal of Atmospheric and Solar-Terrestrial Physics*, *68*(17), 1890–1901. https://doi.org/10.1016/j.jastp.2006.04.004

Qian, L., Burns, A. G., Solomon, S. C., & Wang, W. (2017). Carbon dioxide trends in the mesosphere and lower thermosphere. *Journal of Geophysical Research: Space Physics*, *122*(4), 4474–4488. https://doi.org/10.1002/2016JA023825

Qian, L., Jacobi, C., & McInerney, J. (2019). Trends and solar irradiance effects in the mesosphere. *Journal of Geophysical Research: Space Physics*, *124*(2), 1343–1360. https://doi.org/10.1029/2018JA026367

Rajaram, R., & Gurubaran, S. (1998). Seasonal variabilities of low-latitude mesospheric winds. *Annales Geophysicae*, *16*(2), 197–204. https://doi.org/10.1007/s00585-998-0197-4

Ramesh, K., Smith, A. K., Garcia, R. R., Marsh, D. R., Sridharan, S., & Kishore Kumar, K. (2020a). Long-term variability and tendencies in middle atmosphere temperature and zonal wind from WACCM6 simulations during 1850–2014. *Journal of Geophysical Research: Atmospheres*, *125*(24), e2020JD033579. https://doi.org/10.1029/2020JD033579

Ramesh, K., Smith, A. K., Garcia, R. R., Marsh, D. R., Sridharan, S., & Kishore Kumar, K. (2020b). Long-term variability and tendencies in migrating diurnal tide from WACCM6 simulations during 1850–2014. *Journal of Geophysical Research: Atmospheres*, *125*(23), e2020JD033644. https://doi.org/10.1029/2020JD033644

Ramesh, K., Sridharan, S., & Vijaya Bhaskara Rao, S. (2015). Influence of solar cycle and chemistry on tropical (10°N–15°N) mesopause variabilities. *Journal of Geophysical Research: Space Physics*, *120*(5), 4038–4051. https://doi.org/10.1002/2014JA020930

Randel, W. J., & Wu, F. (1996). Isolation of the ozone QBO in SAGE II data by Singular-value decomposition. *Journal of the Atmospheric Sciences*, *53*(17), 2546–2559. https://doi.org/10.1175/1520-0469(1996)053<2546:IOTOQI>2.0.CO;2

Randel, W. J., & Wu, F. (2007). A stratospheric ozone profile data set for 1979–2005: Variability, trends, and comparisons with column ozone data. *Journal of Geophysical Research*, *112*(D6), D06313. https://doi.org/10.1029/2006JD007339

Rao, S. V. B., Eswaraiah, S., Venkat Ratnam, M., Kosalendra, E., Kishore Kumar, K., Sathish Kumar, S., et al. (2014). Advanced meteor radar installed at Tirupati: System details and comparison with different radars. *Journal of Geophysical Research: Atmospheres*, *119*(21), 11893–11904. https://doi.org/10.1002/2014JD021781

Reed, R. J., Campbell, W. J., Rasmussen, L. A., & Rogers, D. G. (1961). Evidence of a downward-propagating, annual wind reversal in the equatorial stratosphere. *Journal of Geophysical Research*, *66*(3), 813–818. https://doi.org/10.1029/JZ066i003p00813

Rezac, L., Jian, Y., Yue, J., Russell, J. M., Kutepov, A., Garcia, R., et al. (2015). Validation of the global distribution of CO_2 volume mixing ratio in the mesosphere and lower thermosphere from SABER. *Journal of Geophysical Research: Atmospheres*, *120*(23), 12067–12081. https://doi.org/10.1002/2015JD023955

Rind, D., Suozzo, R., Balachandran, N. K., & Prather, M. J. (1990). Climate change and the middle atmosphere. Part I: The doubled CO2 climate. *Journal of the Atmospheric Sciences*, *47*(4), 475–494. https://doi.org/10.1175/1520-0469(1990)047<0475:CCATMA>2.0.CO;2

Salminen, A., Asikainen, T., Maliniemi, V., & Mursula, K. (2020). Dependence of sudden stratospheric warmings on internal and external drivers. *Geophysical Research Letters*, *47*(5), e2019GL086444. https://doi.org/10.1029/2019GL086444

Sassi, F., Kinnison, D., Boville, B. A., Garcia, R. R., & Roble, R. (2004). Effect of El Niño–Southern Oscillation on the dynamical, thermal, and chemical structure of the middle atmosphere. *Journal of Geophysical Research*, *109*(D17), D17108. https://doi.org/10.1029/2003JD004434

Sassi, F., McCormack, J. P., & McDonald, S. E. (2019). Whole atmosphere coupling on intraseasonal and interseasonal time scales: A potential source of increased predictive capability. *Radio Science*, *54*(11), 913–933. https://doi.org/10.1029/2019RS006847

Sathishkumar, S., Sridharan, S., & Jacobi, C. (2009). Dynamical response of low-latitude middle atmosphere to major sudden stratospheric warming events. *Journal of Atmospheric and Solar-Terrestrial Physics*, *71*(8–9), 857–865. https://doi.org/10.1016/j.jastp.2009.04.002

Scaife, A., Guilyardi, E., Cain, M., Gilbert, A., & the RMetS Climate Science Communications Group. (2019). What is the el Niño–southern oscillation? *Weather*, *74*(7), 250–251. https://doi.org/10.1002/wea.3404

Shia, R.-L., Liang, M.-C., Miller, C. E., & Yung, Y. L. (2006). CO_2 in the upper troposphere: Influence of stratosphere-troposphere exchange. *Geophysical Research Letters*, *33*(14), L14814. https://doi.org/10.1029/2006GL026141

Smith, A. K. (2012). Global dynamics of the MLT. *Surveys in Geophysics*, *33*(6), 1177–1230. https://doi.org/10.1007/s10712-012-9196-9

Smith, A. K., Garcia, R. R., Marsh, D. R., & Richter, J. H. (2011). WACCM simulations of the mean circulation and trace species transport in the winter mesosphere. *Journal of Geophysical Research*, *116*(D20), D20115. https://doi.org/10.1029/2011JD016083

Smith, A. K., Pedatella, N. M., Marsh, D. R., & Matsuo, T. (2017). On the dynamical control of the mesosphere–lower thermosphere by the lower and middle atmosphere. *Journal of the Atmospheric Sciences*, *74*(3), 933–947. https://doi.org/10.1175/jas-d-16-0226.1

Sridharan, S., Tsuda, T., & Gurubaran, S. (2007). Radar observations of long-term variability of mesosphere and lower thermosphere winds over Tirunelveli (8.7°N, 77.8°E). *Journal of Geophysical Research*, *112*(D23), D23105. https://doi.org/10.1029/2007JD008669

Sridharan, S., Tsuda, T., & Gurubaran, S. (2010). Long-term tendencies in the mesosphere/lower thermosphere mean winds and tides as observed by medium-frequency radar at Tirunelveli (8.7°N, 77.8°E). *Journal of Geophysical Research*, *115*(D8), D08109. https://doi.org/10.1029/2008JD011609

Venkateswara Rao, N., Espy, P. J., Hibbins, R. E., Fritts, D. C., & Kavanagh, A. J. (2015). Observational evidence of the influence of Antarctic stratospheric ozone variability on middle atmosphere dynamics. *Geophysical Research Letters*, *42*(19), 7853–7859. https://doi.org/10.1002/2015GL065432

Venkateswara Rao, N., Tsuda, T., Riggin, D. M., Gurubaran, S., Reid, I. M., & Vincent, R. A. (2012). Long-term variability of mean winds in the mesosphere and lower thermosphere at low latitudes. *Journal of Geophysical Research*, *117*(A10), A10312. https://doi.org/10.1029/2012JA017850

Vincent, R. A. (2015). The dynamics of the mesosphere and lower thermosphere: A brief review. *Progress in Earth and Planetary Science*, *2*(1), 4. https://doi.org/10.1186/s40645-015-0035-8

Vincent, R. A., Kovalam, S., Fritts, D. C., & Isler, J. R. (1998). Long-term MF radar observations of solar tides in the low-latitude mesosphere: Interannual variability and comparisons with the GSWM. *Journal of Geophysical Research*, *103*(D8), 8667–8683. https://doi.org/10.1029/98jd00482

von Zahn, U., Höffner, J., Eska, V., & Alpers, M. (1996). The mesopause altitude: Only two distinctive levels worldwide? *Geophysical Research Letters*, *23*(22), 3231–3234. https://doi.org/10.1029/96GL03041

Walker, G. T., & Bliss, E. W. (1932). World weather V. *Memoirs Royal Meteorological Society*, *4*, 53–84.

Warner, K., & Oberheide, J. (2014). Nonmigrating tidal heating and MLT tidal wind variability due to the El Niño–Southern Oscillation. *Journal of Geophysical Research: Atmospheres*, *119*(3), 1249–1265. https://doi.org/10.1002/2013JD020407

Wilhelm, S., Stober, G., & Brown, P. (2019). Climatologies and long-term changes in mesospheric wind and wave measurements based on radar observations at high and mid latitudes. *Annales Geophysicae*, *37*(5), 851–875. https://doi.org/10.5194/angeo-37-851-2019

Wilhelm, S., Stober, G., & Chau, J. L. (2017). A comparison of 11-year mesospheric and lower thermospheric winds determined by meteor and MF radar at 69°N. *Annales Geophysicae*, *35*(4), 893–906. https://doi.org/10.5194/angeo-35-893-2017

Wilks, D. S. (2006). *Statistical methods in the atmospheric sciences* (2nd ed.). Academic Press.

Xu, J., Liu, H.-L., Yuan, W., Smith, A. K., Roble, R. G., Mertens, C. J., et al. (2007). Mesopause structure from thermosphere, ionosphere, mesosphere, energetics, and dynamics (TIMED)/Sounding of the atmosphere using broadband emission radiometry (SABER) observations. *Journal of Geophysical Research*, *112*(D9), D09102. https://doi.org/10.1029/2006JD007711

Yamazaki, Y., Matthias, V., Miyoshi, Y., Stolle, C., Siddiqui, T., Kervalishvili, G., et al. (2020). September 2019 Antarctic sudden stratospheric warming: Quasi-6-day wave burst and ionospheric effects. *Geophysical Research Letters*, *47*(1), e2019GL086577. https://doi.org/10.1029/2019GL086577

Younger, J. P., Reid, I. M., Vincent, R. A., Holdsworth, D. A., & Murphy, D. J. (2009). A southern hemisphere survey of meteor shower radiants and associated stream orbits using single station radar observations. *Monthly Notices of the Royal Astronomical Society*, *398*(1), 350–356. https://doi.org/10.1111/j.1365-2966.2009.15142.x

Younger, P. T., Astin, I., Sandford, D. J., & Mitchell, N. J. (2009). The sporadic radiant and distribution of meteors in the atmosphere as observed by VHF radar at Arctic, Antarctic, and equatorial latitudes. *Annales Geophysicae*, *27*(7), 2831–2841. https://doi.org/10.5194/angeo-27-2831-2009

Yue, J., Russell, J., Jian, Y., Rezac, L., Garcia, R., López-Puertas, M., & Mlynczak, M. G. (2015). Increasing carbon dioxide concentration in the upper atmosphere observed by SABER. *Geophysical Research Letters*, *42*(17), 7194–7199. https://doi.org/10.1002/2015GL064696